

FREQUENCY RESPONSE IN SHORT THERMOCOUPLE WIRES

**Final Report
April 1989 - June 1992**

**L. J. Forney
E. L. Meeks
J. Ma**

**Georgia Institute of Technology
Atlanta, Georgia 30332**

**G. C. Fralick
NASA - Lewis Research Center
Cleveland, Ohio 44135**

**Sponsored by
ARNOLD ENGINEERING DEVELOPMENT CENTER
Arnold Air Force Base, Tennessee 37389
under
NASA Cooperative Agreement NCC 3-135**

**Georgia Institute of Technology
October, 1992**

Frequency Response in Short Thermocouple Wires

L. J. Forney¹

E. L. Meeks²

J. Ma³

Georgia Institute of Technology
Atlanta, Georgia 30332

G. C. Fralick

NASA - Lewis Research Center
Cleveland, Ohio 44135

¹ School of Chemical Engineering

² Microelectronics Research Center

³ School of Mechanical Engineering

ABSTRACT

Theoretical expressions are derived for the steady-state frequency response of a thermocouple wire. In particular, the effects of axial heat conduction are demonstrated for a non-uniform wire with unequal material properties and wire diameters across the junction. The amplitude ratio at low frequency $\omega \rightarrow 0$ agrees with the results of Scadron and Warshawsky (1952) for a steady-state temperature distribution. Moreover, the frequency response for a non-uniform wire in the limit of infinite length $l \rightarrow \infty$ is shown to reduce to a simple expression that is analogous to the classic first order solution for a thermocouple wire with uniform properties.

Theoretical expressions are also derived for the steady-state frequency response of a supported thermocouple wire. In particular, the effects of axial heat conduction are demonstrated for both a supported one material wire and a two material wire with unequal material properties across the junction. For the case of a one material supported wire, an exact solution is derived which compares favorably with an approximate expression that only matches temperatures at the support junction. Moreover, for the case of a two material supported wire, an analytical expression is derived that closely correlates numerical results.

Experimental measurements are made for the steady-state frequency response of a supported thermocouple wire. In particular, the effects of axial heat conduction are demonstrated for both a supported one material wire (type K) and a two material wire (type T) with unequal material properties across the junction. The data for the amplitude ratio and phase angle are correlated to within 10% with the theoretical predictions of Forney and Fralick (1991). This is accomplished by choosing a natural frequency ω_n for the wire data to correlate the first order response at large gas temperature frequencies. It is found that a large bead size, however, will increase the amplitude ratio at low frequencies but decrease the natural frequency of the wire. The phase angle data are also distorted for imperfect junctions.

PREFACE

The work reported herein was sponsored by the Air Force Systems Command (AFSC) under NASA cooperative agreement NCC 3-135 for the Arnold Engineering Development Center (AEDC), AFSC, Arnold Air Force Station, Tennessee. The contract officers are Ms. Marjorie Collier and Captain Hal Martin for the Directorate of Technology (DOT), AFSC. The authors also wish to acknowledge the support of Dr. W. D. Williams, head of the Research Sensor Technology Branch of NASA-Lewis.

TABLE OF CONTENTS

	<u>Page</u>
1.0 UNSUPPORTED THERMOCOUPLE WIRE: THEORY	3
1.1 INTRODUCTION	3
1.2 THEORY	4
1.2.1 Uniform Wire	
1.2.2 Previous Work	
1.2.3 Non-Uniform Wire	
1.3 RESULTS	13
1.3.1 Uniform Wire	
1.3.2 Non-Uniform Wire	
1.4 NOMENCLATURE	20
1.5 REFERENCES	23
1.6 TABLES AND FIGURES	24
2.0 SUPPORTED THERMOCOUPLE WIRE: THEORY AND EXPERIMENT	38
2.1 INTRODUCTION	38
2.2 THEORY FOR ONE MATERIAL THERMOCOUPLE	39
2.2.1 Approximate Solution	
2.2.2 Exact Solution	
2.3 THEORY FOR TWO MATERIAL THERMOCOUPLE	46
2.3.1 Temperature Distribution for Small Wire	
2.3.2 Temperature Distribution for Large Wire	
2.3.3 Frequency Response	
2.4 RESULTS	49
2.4.1 One Material Thermocouple	
2.4.2 Two Material Thermocouple	
2.5 EXPERIMENTAL PROCEDURE	54
2.5.1 Rotating Wheel Experiment	
2.5.2 Thermocouple Construction	
2.5.3 Asyst Software	

1.0 UNSUPPORTED THERMOCOUPLE WIRE: THEORY

Theoretical expressions are derived for the steady-state frequency response of a thermocouple wire. In particular, the effects of axial heat conduction are demonstrated for a non-uniform wire with unequal material properties and wire diameters across the junction. The amplitude ratio at low frequency $\omega \rightarrow 0$ agrees with the results of Scadron and Warshawsky for a steady-state temperature distribution. Moreover, the frequency response for a non-uniform wire in the limit of infinite length $l \rightarrow \infty$ is shown to reduce to a simple expression that is analogous to the classic first order solution for a thermocouple wire with uniform properties.

1.1 INTRODUCTION

The measurement of fluctuating temperatures in the high speed exhaust of a gas turbine engine combustor is required to characterize the local gas density gradients or convective heat transfer (Fralick, 1985). Although thermocouples are suitable for the measurement of high frequency temperature fluctuations (< 1 KHz) in a flowing gas or liquid, the measured signal must be compensated since the frequency of the time dependent fluid temperature is normally much higher than the corner frequency of the thermocouple probe (Scadron and Warshawsky, 1952). Moreover, the amplitude and phase angle of the thermocouple response may be attenuated by axial heat conduction for rugged thermocouples of finite length (Elmore, et al.; 1983, 1986).

1.2.1 Uniform Wire

In this section the geometry of Fig. 1 is considered where the material properties of thermal conductivity k , specific heat c and wire density ρ are assumed to be equal on both sides of the thermocouple junction. If the probe is subjected to a flowing fluid, whose temperature fluctuates about its mean, the expression for the local conservation of energy in the thermocouple wire becomes (Scadron and Warshawsky, 1952)

$$\frac{\partial T_w}{\partial t} = \alpha \frac{\partial^2 T_w}{\partial x^2} + \frac{4h}{\rho c D} (T_g - T_w) \quad (1.1)$$

where $\alpha = k / \rho c$ is the thermal diffusivity of the wire, T_g is the ambient fluid temperature, h is the convective heat transfer coefficient, D is the wire diameter and T_w is the local wire temperature measured along the axis at a distance x from the centerline of Fig. 1.

If the wire and fluid temperatures are measured relative to the support and mean fluid temperature T_0 , the variation in the ambient fluid temperature can be written in the complex form

$$T_g(t) = T_0 + T_f e^{i\omega t} \quad (1.2)$$

where ω is the angular frequency of the ambient fluid. Since Eq. (1.1) is linear, we now seek a solution for the local wire temperature of the form (Hildebrand, 1976)

$$T_w = T_0 + \vec{T}_\omega(x) e^{i\omega t}. \quad (1.3)$$

Referencing all temperatures with respect to the steady-state temperature T_0 and normalizing with respect to the amplitude of the fluctuating ambient fluid

where the constants A and B are complex, $1/G(\omega)$ represents the particular solution and the parameter

$$q = \sqrt{\frac{G(\omega)}{\gamma}}$$

Substituting $x = \pm l$ in Eq. (1.9), the boundary condition Eq. (1.7) yields values for the constants

$$A = 0, B = \frac{-1}{G(\omega) \cosh ql}. \quad (1.10)$$

Hence, one obtains a steady-state frequency response for the simple uniform wire of Fig. 1 in the form (Forney, 1988)

$$T = \frac{1}{G(\omega)} \left(1 - \frac{\cosh qx}{\cosh ql}\right) \quad (1.11)$$

The steady-state frequency response at the junction $x = 0$ of fig. 1 now becomes

$$T(0) = \frac{1}{G(\omega)} (1 - \operatorname{sech} ql). \quad (1.12)$$

The term $1 - \operatorname{sech} (ql)$ in Eq. (1.12) corresponds to the steady-state temperature distribution for a constant ambient fluid temperature $T_f > T_o$ derived by Scadron and Warshawsky (1952). It is also interesting to note that the first order response can be derived from Eq. (1.12) in the limit of large wire length l or

$$\lim_{l \rightarrow \infty} T(0) = \frac{1}{G(\omega)} \quad (1.13)$$

where Eq. (1.13) represents the frequency response of a uniform thermocouple wire with no axial heat conduction.

$$S_1 = 1 - \sum_{j=1}^{\infty} c_j \left[\frac{d_j(d_j - 1)}{d_j^2 + \left(\frac{\omega}{\omega_n}\right)^2} \right] \quad (1.18a)$$

and

$$S_2 = \sum_{j=1}^{\infty} c_j \left[\frac{d_j - 1}{d_j^2 + \left(\frac{\omega}{\omega_n}\right)^2} \right] \quad (1.18b)$$

where the constant that appear in the terms of S_1 and S_2 are

$$c_j = \frac{2}{j\pi} [1 - \cos(j\pi)] \sin\left(\frac{j\pi(1-x)}{2l}\right) \quad (1.19a)$$

and

$$d_j = 1 + \frac{(j\pi)^2 \gamma}{4l^2}. \quad (1.19b)$$

Properties of these solutions derived by Scadron and Warshawsky are discussed in Sec. III.

1.2.3 Non-Uniform Wire

If the wire diameters or the physical properties such as thermoconductivity are different across the thermocouple junction as shown in fig.2, Eq.(1.6) must be solved in the separate regions 1 and 2 on both sides of the junction. This solution is subject to the boundary conditions of continuous temperature and equal rates of conductive heat transfer at the junction $x = 0$ or

$$T_1(-l) = T_2(l) = 0 \quad (1.20a)$$

$$T_1(0) = T_2(0) \quad (1.20b)$$

Similarly, substituting Eqs. (1.22) and (1.23) into boundary condition (1.20c), one obtains a second linear equation for A_1, A_2 or

$$A_1 Q \cosh q_1 l + A_2 \cosh q_2 l = R_2 . \quad (1.25)$$

Here, the complex constant

$$Q = (k_1 D_1^2 q_1) / (k_2 D_2^2 q_2) \quad (1.26)$$

and the complex constants R_1, R_2 are equal to

$$R_1 = \left(\frac{1}{G_2} - \frac{1}{G_1} \right) + \frac{1}{G_1} \cosh q_1 l - \frac{1}{G_2} \cosh q_2 l \quad (1.27)$$

and

$$R_2 = \frac{Q}{G_1} \sinh q_1 l + \frac{1}{G_2} \sinh q_2 l. \quad (1.28)$$

Solving Eqs. (1.24) and (1.25) for A_1 and A_2 , one obtains the determinate system

$$A_1 = \frac{\begin{vmatrix} R_1 & -\sinh q_2 l \\ R_2 & \cosh q_2 l \end{vmatrix}}{DET} \quad (1.29)$$

$$A_2 = \frac{\begin{vmatrix} \sinh q_1 l & R_1 \\ Q \cosh q_1 l & R_2 \end{vmatrix}}{DET} \quad (1.30)$$

where the determinate in the denominator is equal to

$$DET = \sinh q_1 l \cosh q_2 l + Q \cosh q_1 l \sinh q_2 l \quad (1.31)$$

Thus, the constants A_1 and A_2 in Eqs. (1.22) and (1.23) become

$$A_1 = \frac{\frac{\sinh q_1 l}{G_1} \left(\tanh \frac{q_1 l}{2} + Q \tanh q_2 l \right) + \frac{\sinh q_2 l}{G_2} \left(-\tanh \frac{q_2 l}{2} + \tanh q_2 l \right)}{\sinh q_1 l + Q \cosh q_1 l \tanh q_2 l} \quad (1.32)$$

and

1.3 RESULTS

The amplitude ratio and phase angle of the thermocouple frequency response were plotted graphically for the case of a uniform wire with the geometry shown in fig. 1. In this case, average properties of a type B or *Pt / 6% Rh – Pt / 30% Rh* were used since the material properties were nearly equal across the thermocouple junction. The wire dimensions, properties and gas conditions are listed in table 1 (Touloukian et al., 1970).

The amplitude ratio and phase angle were also plotted for a composite or non-uniform thermocouple wire with the geometry shown in fig. 2. In this case, different wire diameters and material properties were used including a type B thermocouple described in Table 1 in addition to a type T or copper - constantan described in table 2 (Touloukian et al., 1970).

The form of the convective heat transfer coefficient h that appears in the computation of the natural frequency ω_n defined in Eq. (1.8) was determined from the expression (Scadron and Warshawsky 1952)

$$Nu = .431 Re^{1/2} \quad (1.36)$$

where $Nu (= hD / k_f)$ is the Nusselt number, k_f is the thermal conductivity of the ambient fluid and $Re (= v D / \nu_f)$ is the Reynolds number of the thermocouple wire. Here, v and ν_f are the fluid velocity and kinematic viscosity, respectively. It should be noted that the convective heat transfer coefficient $h \propto D^{1/2}$ and the natural frequency of a thermocouple wire for given material properties

$$\omega_n \propto D^{-3/2}.$$

The phase angle Φ for all three theories is computed in fig. 4. The phase angle varies over the range $0 \geq \Phi \geq -\pi/2$ and approaches the lower limit of $-\pi/2$ for large frequencies $\omega / \omega_n \gg 1$. It is apparent that the effect of axial heat conduction is to reduce the magnitude of the phase angle.

The spacial variation of the amplitude ratio $|T(x)|$ derived from Eq. (1.11) is graphed in fig. 5. The present theory approaches the correct limit of $|T(\pm l)| = 0$. However, the theory of Scadron and Warshawsky oscillates near the end of the wire $x \rightarrow \pm l$. In the latter case the amplitude ratio equals the value

$1 / \sqrt{1 + (\omega / \omega_n)^2}$ for $x = \pm l$ since $S_1 = 1$ and $S_2 = 0$ in Eqs. (1.18a) and (1.18b), respectively. An incorrect value for the amplitude ratio near the ends of the wire would not ordinarily present a problem unless one wished to adapt the theory to the common configuration of a supported thermocouple wire with heat transfer down the support legs (Forney and Fralick, 1991).

1.3.2 Non-Uniform Wire

The amplitude ratio $|T_1(0)|$ from the steady-state frequency response Eq. (1.34) is graphed in fig. 6. This plot assumes a type T thermocouple wire with the dimensions listed in table 2. An important parameter that affects the relative magnitude of the terms in Eq. (1.34) and thus the relative importance of the thermocouple wire segments in regions 1 or 2 in the schematic of fig. 2 is the complex dimensionless ratio $Q = k_1 D_1^2 q_1 / k_2 D_2^2 q_2$. We note here that Q assumes different values in the limit of either low or high frequencies. Given that the Nusselt number is related to the wire Reynolds number by Eq. (1.36), one obtains

The amplitude ratio $|T_1(0)|$ from Eq. (1.35) for a type T thermocouple wire with the same wire dimensions $D_2 / D_1 = 2$ as the solid curve in fig. 6 but of infinite length $l \rightarrow \infty$ is also computed. As indicated, the amplitude ratio at low frequencies $\omega \rightarrow 0$ for a non-uniform thermocouple wire of infinite length approaches $|T_1(0)| \rightarrow 1$. This result is identical to the first order frequency response Eq. (1.13) for a uniform wire of infinite length as is shown in fig. 3. For the non-uniform wire, however, axial heat transfer does occur at the junction because of dissimilar material properties. At large frequencies $\omega / \omega_n \gg 1$, however, the amplitude ratio derived from Eq. (1.35) for the wire of infinite length asymptotically approaches the value predicted by Eq. (1.34) for a wire of finite length as shown in fig. 6. The latter result is similar to the features of fig. 3 at large frequencies for the case of a uniform thermocouple wire. These latter features reflect the fact that the time scales of the ambient gas temperature fluctuations at high frequency are too small for axial heat conduction to occur.

The phase angle Φ for both expressions Eqs. (1.34) and (1.35) is graphed in fig. 7. The phase angle varies over the range $0 \geq \Phi \geq -\pi/2$ and approaches the lower limit of $-\pi/2$ for large frequencies. It is apparent that the effect of axial heat conduction is to reduce the magnitude of the phase angle.

The amplitude ratio $|T_1(0)|$ derived from Eq. (1.34) for a type B thermocouple wire is computed in fig. 8. Since the material properties in this case are nearly equal on both sides of the junction, the indicated difference in the amplitude ratio is the result of different wire diameters across the junction. These results are strongly influenced by the magnitude of the factor Q_0 defined by Eq. (1.37). If

The amplitude ratio $|T_1(x)|$ is also computed as a function of the axial distance down the type T thermocouple wire in fig. 13. As discussed above, $Q_0 > 1$ for both wire configurations. Thus, the large rate of axial heat transfer down the copper wire in region 1 gives nearly equal spacial temperature profiles for both wire configurations and this fixes the junction temperature.

S_2	=	infinite sum
t	=	time(s)
T	=	frequency response
T_f	=	amplitude of periodic gas temperature ($^{\circ}K$)
T_g	=	gas temperature ($^{\circ}K$)
T_0	=	steady-state gas temperature ($^{\circ}K$)
\vec{T}_ω	=	complex amplitude of periodic wire temperature($^{\circ}K$)
T_w	=	local wire temperature ($^{\circ}K$)
v	=	gas velocity ($cm - s^{-1}$)
x	=	axial distance from center of wire (cm)

Greek Symbols

α	=	thermal diffusivity ($cm^2 - s^{-1}$)
γ	=	α / ω_n (cm^2)
γ^+	=	$1/\sqrt{\gamma_1} + 1/\sqrt{\gamma_2}$ (cm^{-1})
γ^-	=	$1/\sqrt{\gamma_1} - 1/\sqrt{\gamma_2}$ (cm^{-1})
ν_f	=	kinematic viscosity of gas ($cm^2 - s^{-1}$)
ω	=	angular frequency (s^{-1})
ω_n	=	natural frequency of wire ($= 4h / \rho c D$)(s^{-1})
Φ	=	phase angle (degrees)

1.5 REFERENCES

1. Carslaw, H. S., Introduction to the Mathematical Theory of the Conduction of Heat in Solids, Dover Publications, 2nd edition (1945).
2. Dils, R. R. and Follansbee, P. S., Wide Bandwidth Gas Temperature Measurements in Combustor and Combustor Exhaust Gases, Instrumentation in the Aerospace Industry, 21 (B. Washburn, ed.), ISA 76245 (1976).
3. Elmore, D. L., Robinson, W. W. and Watkins, W. B., Dynamic Gas Temperature Measurement System: Final Report, NASA CR-168267 (1983).
4. Elmore, D.L., Robinson, W. W. and Watkins, W. B., Further Development of the Dynamic Gas Temperature Measurement System: Vol. I - Technical Efforts, NASA CR-179513 (1986).
5. Forney, L. J., Frequency Response of a Thermocouple Wire: Effects of Axial Conduction, NASA/ASEE Case-Lewis Summer Faculty Fellowship Program, 1988 Final Report, pp. 78-79.
6. Fralick, G. C., Correlation of Velocity and Velocity-Density Turbulence in the Exhaust of an Atmospheric Burner, Turbine Engine Hot Section Technology - 1985, NASA CP-2465, pp. 81-85.
7. Forney, L. J., and Fralick, G. C., Frequency Response of a Supported Thermocouple Wire: Effects of Axial Heat Conduction, Progress Report Georgia Tech E19-666-2, April (1991).
8. Hildebrand, F. B., Advanced Calculus for Applications, (2nd Ed), Prentice - Hall (1976).
9. Scadron, M.D. and Warshawsky, I., Experimental Determination of Time Constants and Nusselt Numbers for Bare-Wire Thermocouples in High-Velocity Air Streams and Analytic Approximation of Conduction and Radiation Errors, NACA TN-2599 (1952).
10. Touloukian, Powell, Ho and Clemens, (ed.), Thermal Physical Properties of Matter, Purdue Research Foundation, Plenum Pub. (1970).

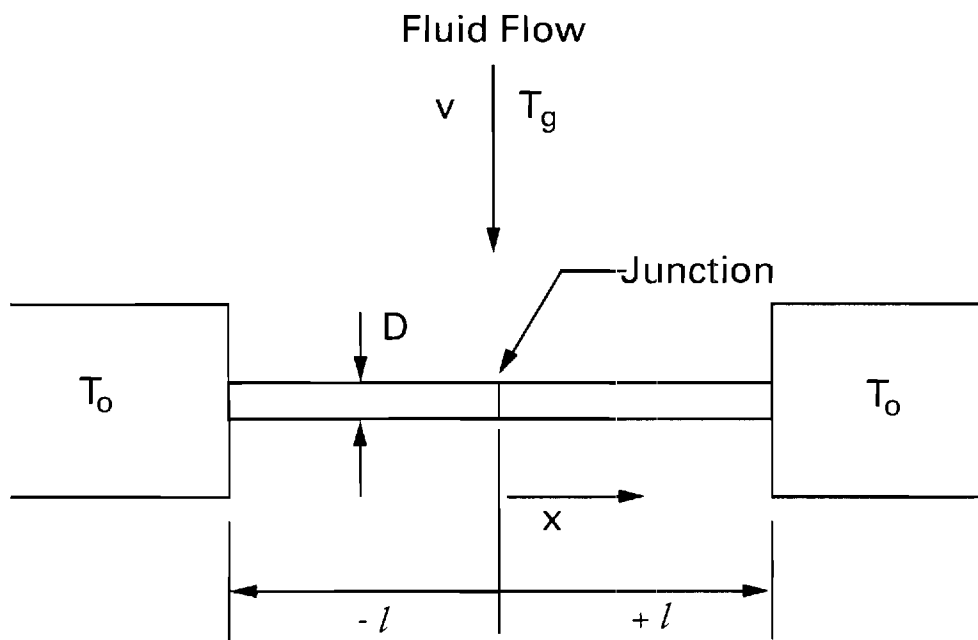


Fig. 1 Schematic of uniform wire

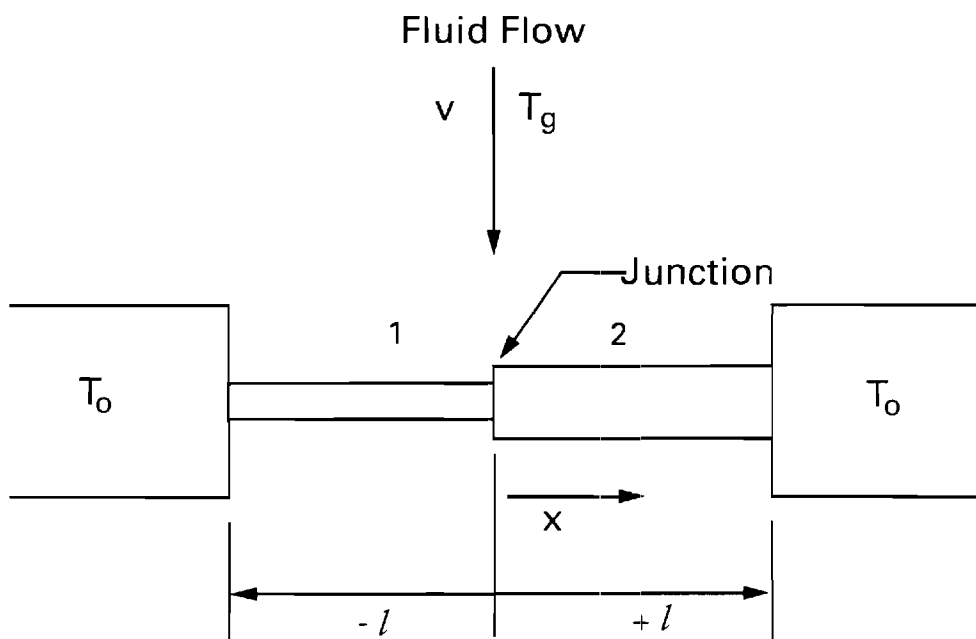


Fig. 2 Schematic of non-uniform wire

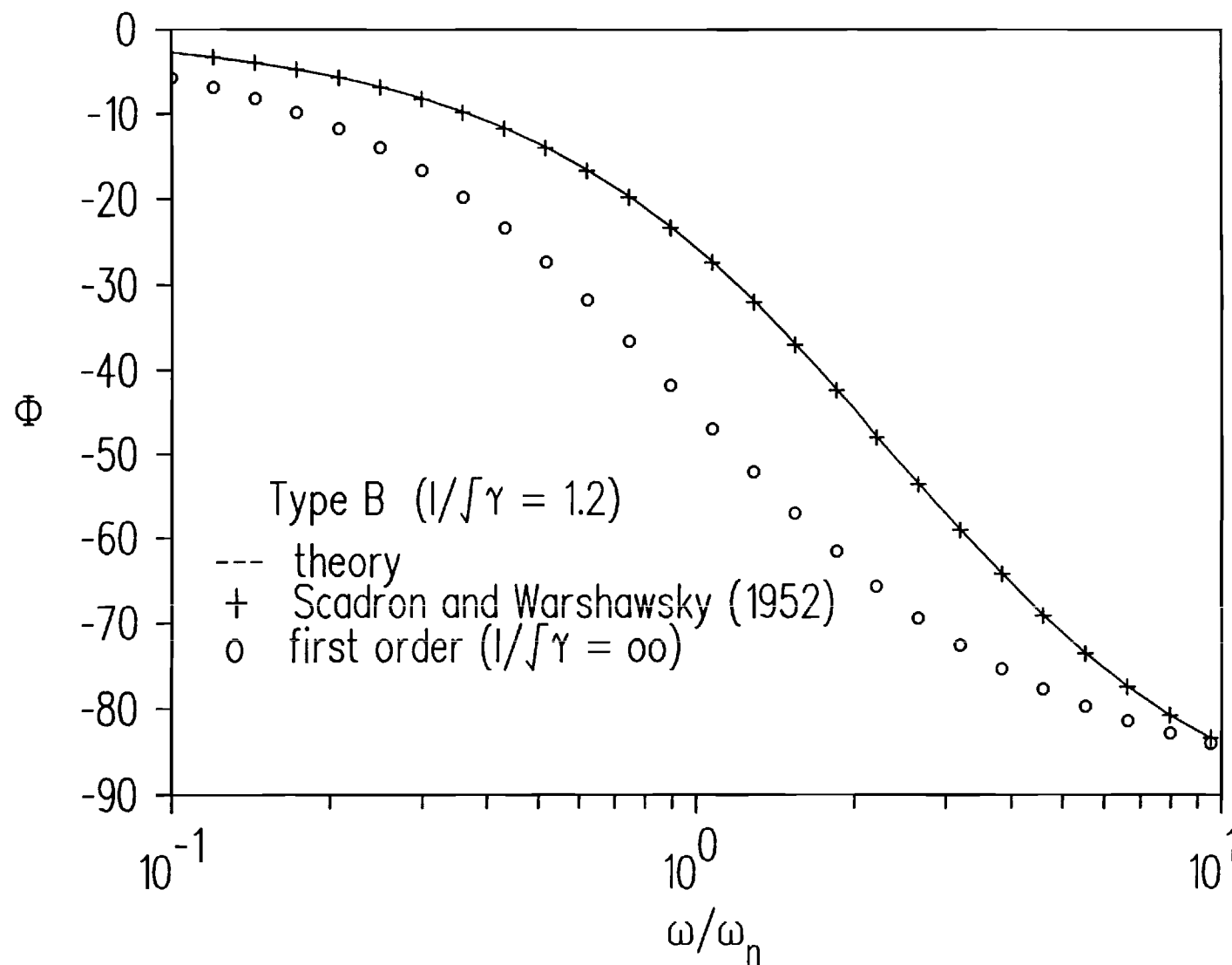


Fig. 4 Phase angle vs angular frequency for uniform wire.
 Solid line, Eq. (12); Circles, Eq. (13).

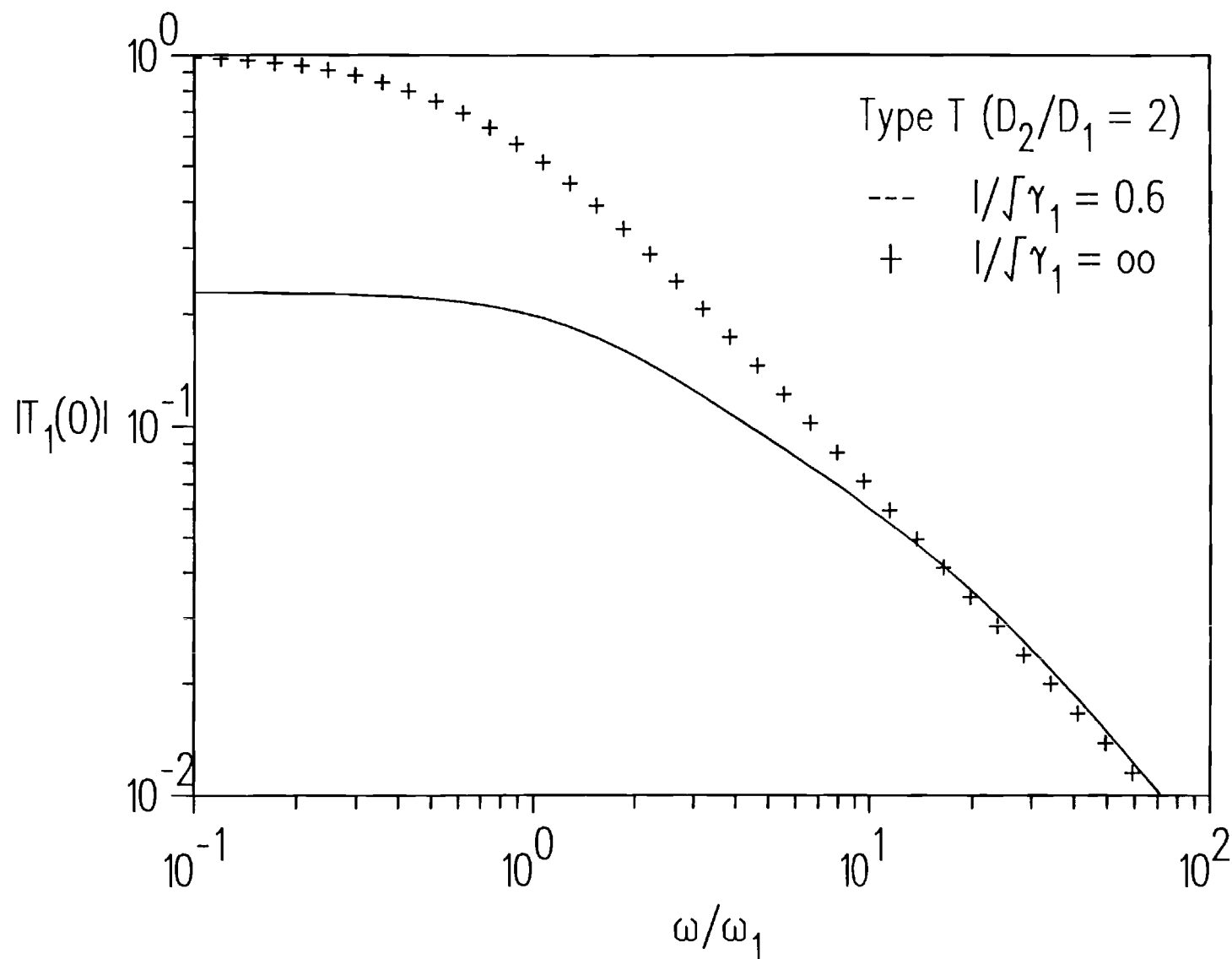


Fig. 6 Amplitude ratio vs angular frequency for non-uniform wire. Upper curve is Eq. (35). Lower curve is Eq. (34).

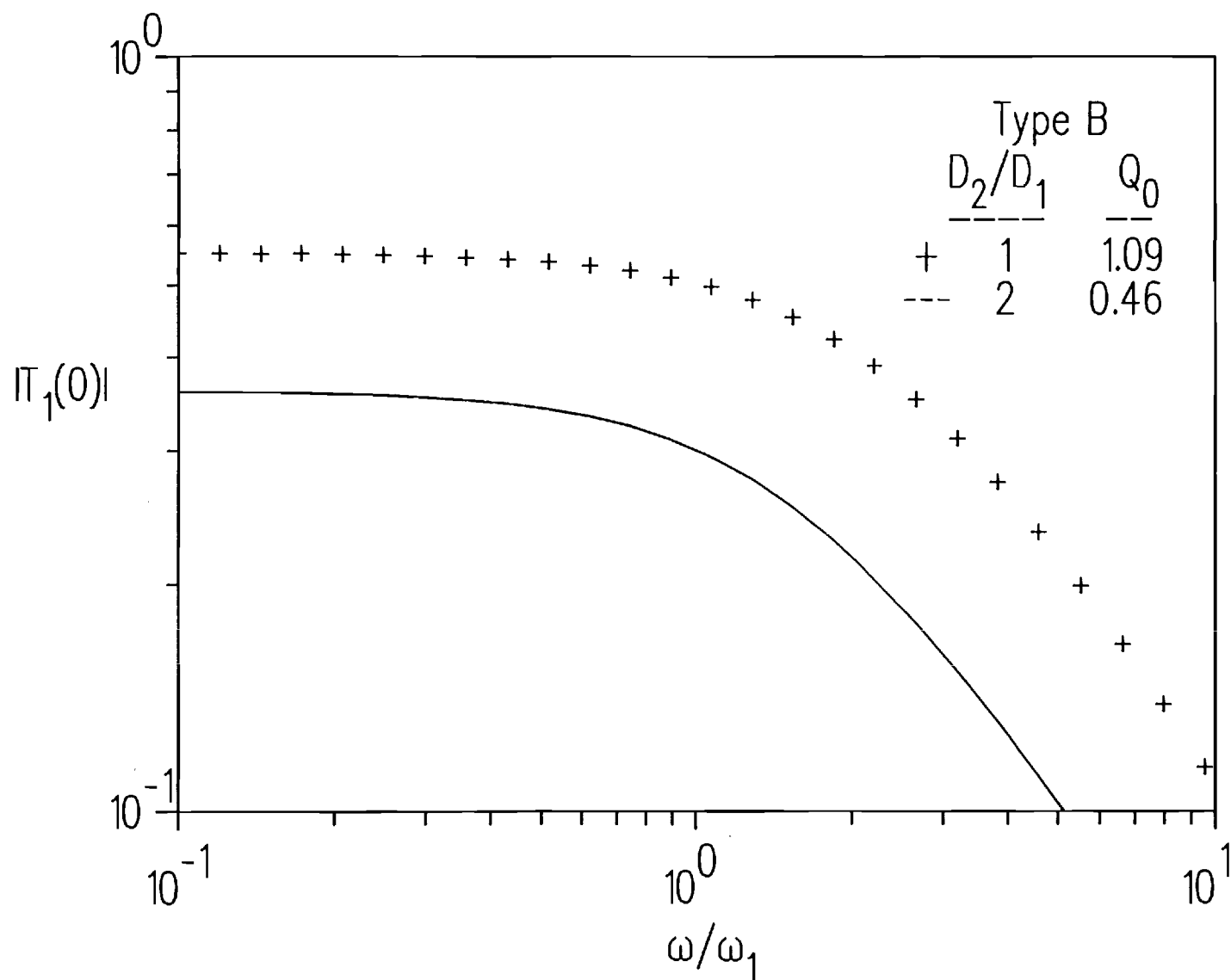


Fig. 8 Amplitude ratio vs angular frequency for non-uniform wire with similar material properties. Curves are Eq. (34).

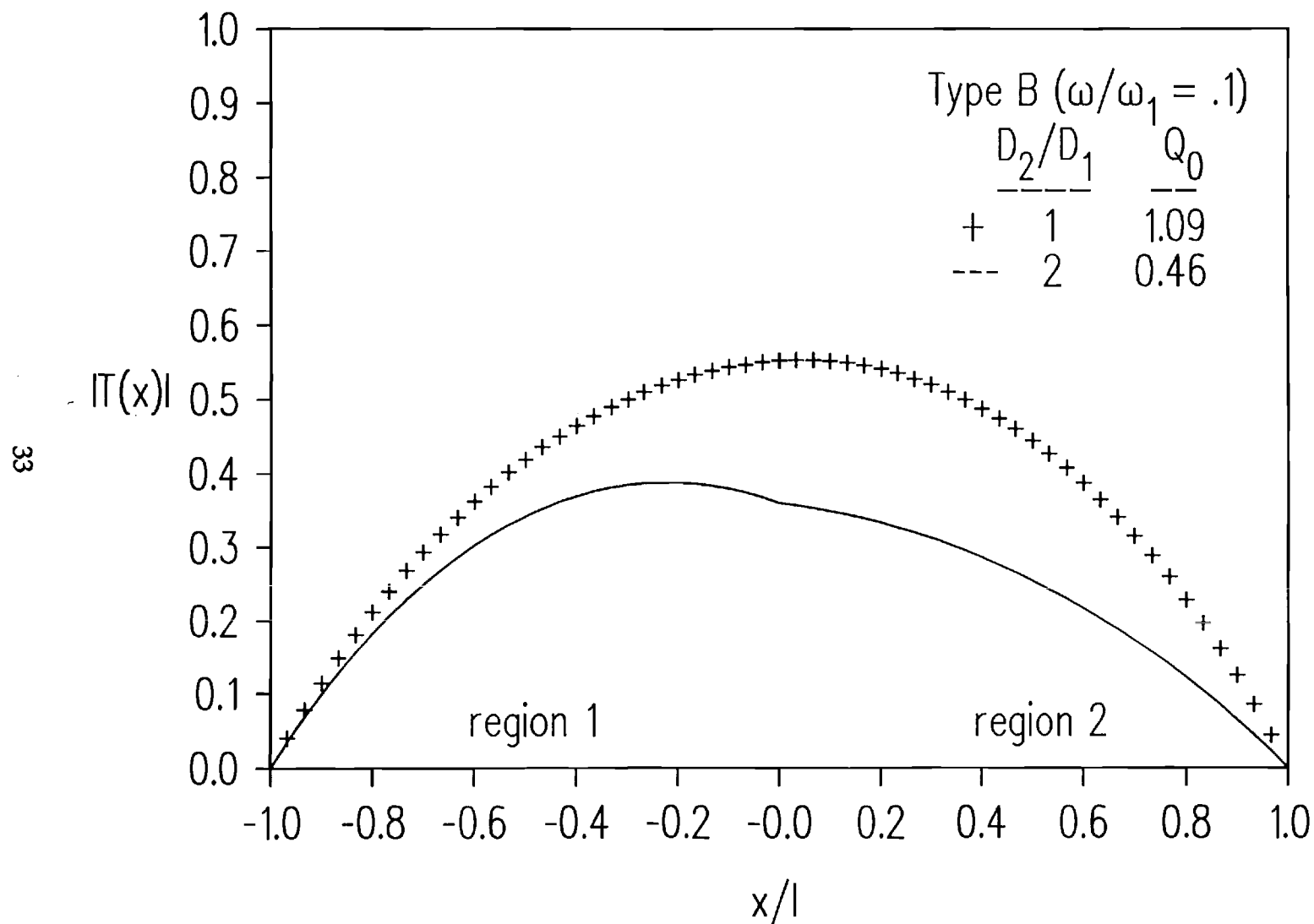


Fig. 10 Amplitude ratio vs axial distance for non-uniform wire with similar material properties. Each curve is derived from Eqs. (22) and (32).

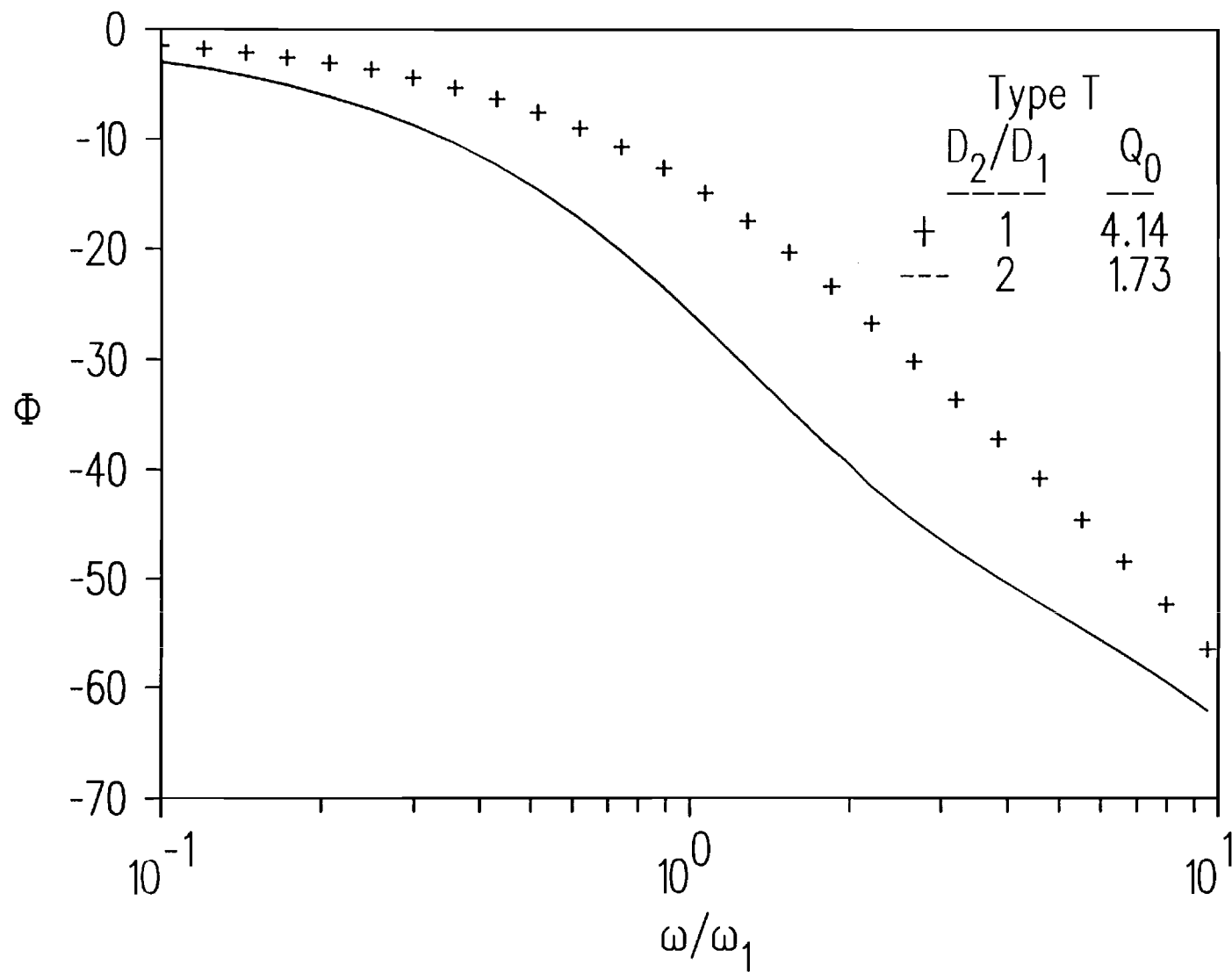


Fig. 12 Phase angle vs angular frequency for wire with dissimilar material properties. Curves derived from Eq. (34).

2.2 THEORY FOR ONE MATERIAL THERMOCOUPLE

The steady-state frequency response of a thermocouple wire will be developed with the following assumptions: (a) the amplitude of the fluctuating fluid temperature is small relative to the mean absolute temperature (b) the thermocouple dimensions are small relative to the size of the turbulent eddies or enclosure dimensions (c) radial temperature gradients in a wire cross section can be neglected and (d) radiative heat transfer can be neglected relative to conduction and convection.

In this section the geometry of Fig. 1 is considered where the material properties of thermal conductivity k , specific heat c and wire density ρ are assumed to be equal on both sides of the thermocouple junction. If the probe is immersed in a flowing fluid, the expression for the local conservation of energy in the thermocouple wire becomes (Scadron and Warshawsky, 1952)

$$\frac{\partial T_w}{\partial t} = \alpha \frac{\partial^2 T_w}{\partial x^2} + \frac{4h}{\rho c D} (T_g - T_w) \quad (2.1)$$

where $\alpha = k / \rho c$ is the thermal diffusivity of the wire, T_g is the ambient fluid temperature, h is the convective heat transfer coefficient, D is the wire diameter and T_w is the local wire temperature measured along the axis at a distance x from the centerline (Fig. 1.)

The wire and fluid temperatures are measured relative to the mean fluid temperature T_0 . The ambient fluid temperature is taken to be a mean temperature together with a sinusoidal varying deviation from the mean,

$$T_g(t) = T_0 + T_f e^{i\omega t} \quad (2.2)$$

where ω is the angular frequency of the ambient temperature. Since Eq. (2.1) is

while in Eq. (2.7) the constants A and B are complex, $1/G(\omega)$ represents the particular solution and the parameter

$$q = \sqrt{\frac{G(\omega)}{\gamma}}.$$

2.2.1 Approximate Solution

Assuming that the material properties are constant across the junction and that the wire diameters are D_1 and D_2 in regions 1 and 2, respectively, Eq. (2.6) is subject to the boundary conditions

$$T_1(l) = T_2(l) = T_a \quad (2.9a)$$

$$T_2(l+L) = 0 \quad (2.9b)$$

In this case, we seek a simple approximate solution that neglects the heat transfer at the interface between regions 1 and 2 at $x = \pm l$ where the parameters in Eqs. (2.5) and (2.6) are defined in terms of the wire diameters in each region. A similar approach will be used in a later section to obtain an approximate solution for the case in which the material properties of the two elements of the thermocouple are distinctly different. Hence, in region 1

$$\omega_1 = \frac{4h_1}{\rho c D_1}, \quad \gamma = \frac{\alpha}{\omega_1}, \quad G_1(\omega) = 1 + i\left(\frac{\omega}{\omega_1}\right) \quad (2.0)$$

where ω_1 is the natural frequency of the wire in region 1 of fig. 1.

The solution to Eq. (2.6) for the one material wire on both sides of the junction in region 1 can be written in the form

$$T_1(x) = A_1 \sinh q_1 x + B_1 \cosh q_1 x + \frac{1}{G_1(\omega)} \quad (2.11)$$

$$T_1(0) = \frac{1}{G_1} \left(1 - \frac{1}{\cosh q_1 l} \right) + \frac{1}{G_2} \left(1 - \frac{\cosh q_2 l}{\cosh q_2 (l+L)} \right) \frac{1}{\cosh q_1 l} \quad (2.17)$$

The steady-state frequency at the thermocouple junction $x=0$ is normally characterized graphically in the form

$$T(0) = |T(0)|e^{i\Phi} \quad (2.18)$$

where $|T(0)|$ is the amplitude ratio and Φ is the phase angle. In the latter case, the phase angle in degrees is

$$\Phi = 57.3 \tan^{-1} \left[\frac{\text{Im } T(0)}{\text{Re } T(0)} \right] \quad (2.19)$$

where $\text{Im}[T(0)]$ and $\text{Re}[T(0)]$ are the imaginary and real parts of $T(0)$, respectively.

2.2.2 Exact Solution

If the boundary conditions listed in Eq.(2.9) include equal rates of conductive heat transfer at the interface between the thermocouple and support wires at $x = \pm l$, the exact solution is subject to

$$T_1(l) = T_2(l) \quad (2.20a)$$

$$kD_1^2 \frac{dT_1(l)}{dx} = kD_2^2 \frac{dT_2(l)}{dx} \quad (2.20b)$$

$$T_2(l+L) = 0 \quad (2.20c)$$

Since the solution to Eq. (2.6) in region 1 is of the form

$$T_1(x) = A_1 \sinh q_1 x + B_1 \cosh q_1 x + \frac{1}{G_1} \quad (2.21)$$

where by symmetry $T_1(l) = T_1(-l)$, one obtains $A_1 = 0$. Thus, the form of the

$$B_1 = \frac{\begin{vmatrix} \frac{1}{G_2}[1 - \cosh q_2 L] - \frac{1}{G_1} & -\sinh q_2 L \\ \frac{1}{G_2} \sinh q_2 L & \cosh q_2 L \end{vmatrix}}{DET} \quad (2.28)$$

and

$$A_2 = \frac{\begin{vmatrix} \cosh q_1 l & \frac{1}{G_2}[1 - \cosh q_2 L] - \frac{1}{G_1} \\ Q \sinh q_1 l & \frac{1}{G_2} \sinh q_2 L \end{vmatrix}}{DET} \quad (2.29)$$

where the determinate in the denominator is equal to

$$DET = \cosh q_1 l \cosh q_2 L + Q \sinh q_1 l \sinh q_2 L. \quad (2.30)$$

Thus, solving for the constants B_1 and A_2 from Eqs. (2.28) and (2.29) and substituting B_1 into Eq. (2.22), one obtains an exact expression for the steady-state temperature distribution in the form

$$T_1(x) = \frac{\left[\frac{1}{G_2}(\cosh q_2 L - 1) - \frac{1}{G_1} \cosh q_2 L \right] \cosh q_1 x}{\cosh q_1 l \cosh q_2 L + Q \sinh q_1 l \sinh q_2 L} + \frac{1}{G_1}. \quad (2.31)$$

Thus, the steady-state frequency response at the thermocouple junction $x=0$ becomes

$$T(0) = \frac{\frac{1}{G_2}(\cosh q_2 L - 1) - \frac{1}{G_1} \cosh q_2 L}{\cosh q_1 l \cosh q_2 L + Q \sinh q_1 l \sinh q_2 L} + \frac{1}{G_1}. \quad (2.32)$$

$$T_1(0) = T_2(0) \quad (2.35a)$$

$$k_1 D_1^2 \frac{dT_1(0)}{dx} = k_2 D_1^2 \frac{dT_2(0)}{dx} \quad (2.35b)$$

$$T_1(-l) = T_a \quad (2.35c)$$

$$T_2(l) = T_b \quad (2.35d)$$

Solving for the four values of the constants designated by A and B in Eqs. (2.33) and (2.34), one obtains an expression for the steady-state temperature distribution in region 1 of the form

$$\begin{aligned} T_1(x) = & \frac{1}{G_1} + \left\{ \sinh q_1(x+l) \left[\left(\frac{1}{G_2} - \frac{1}{G_1} \right) \cosh q_2 l + \left(T_b - \frac{1}{G_2} \right) \right] \right. \\ & \left. + \left(T_a - \frac{1}{G_1} \right) \left[Q_t \cosh q_1 x \sinh q_2 l - \sinh q_1 x \cosh q_2 l \right] \right\} \left(\frac{1}{\Delta_1} \right) \end{aligned} \quad (2.36a)$$

and in region 2

$$\begin{aligned} T_2(x) = & \frac{1}{G_2} + \left\{ -Q_t \sinh q_2(l-x) \left[\left(\frac{1}{G_2} - \frac{1}{G_1} \right) \cosh q_1 l - \left(T_a - \frac{1}{G_1} \right) \right] \right. \\ & \left. + \left(T_b - \frac{1}{G_2} \right) \left[\cosh q_2 x \sinh q_1 l + Q_t \cosh q_1 l \sinh q_2 x \right] \right\} \left(\frac{1}{\Delta_1} \right). \end{aligned} \quad (2.36b)$$

Here, it should be noted that the two functions above can be obtained from each other by interchanging the subscripts 1 and 2, the values a and b and by changing the sign of x. Also, in Eqs. (2.36a) and (2.36b) the parameters

$$\Delta_1 = Q_t \cosh q_1 l \sinh q_2 l + \cosh q_2 l \sinh q_1 l$$

and

$$Q_t = \frac{k_1 q_1}{k_2 q_2}.$$

and

$$T_b = \frac{1}{G_4} + \left\{ Q_s \sinh q_4 L \left[\left(\frac{1}{G_3} - \frac{1}{G_4} \right) \cosh q_3(l+L) - \frac{1}{G_3} \right] - \frac{1}{G_4} [\cosh q_4 l \sinh q_3(l+L) + Q_s \cosh q_3(l+L) \sinh q_4 l] \right\} \left(\frac{1}{\Delta_2} \right). \quad (2.39)$$

Here, the parameters are defined as

$$\Delta_2 = Q_s \cosh q_3(l+L) \sinh q_4(l+L) + \cosh q_4(l+L) \sinh q_3(l+L)$$

and

$$Q_s = \frac{k_1 q_3}{k_2 q_4}.$$

2.3.3 Frequency Response

The steady-state frequency response for the two material supported thermocouple is obtained from Eq. (2.36a) or (2.36b) by setting $x = 0$:

$$T(0) = \frac{1}{\Delta_1} \left\{ Q_s \sinh q_2 l \left[T_a + \frac{1}{G_1} (\cosh q_1 l - 1) \right] + \sinh q_1 l \left[T_b + \frac{1}{G_2} (\cosh q_2 l - 1) \right] \right\} \quad (2.40)$$

where T_a and T_b are given by Eqs. (2.38) and (2.39).

It should be noted that the steady-state frequency response Eq. (2.40) provides a wire temperature that is continuous everywhere and conserves the heat flux at the junction $x = 0$. This represents an approximate solution since the heat flux at the interface between the large and small wires $x = \pm l$ has been neglected.

2.4 RESULTS

The amplitude ratio and phase angle of the thermocouple frequency response were plotted graphically for the case of a one material wire as shown in the

B thermocouple wire with the dimensions listed in table 1. In this case, the average material properties listed in table 1 were used since the one material theory assumes that the properties of the thermocouple wire are uniform across the junction. It is evident in fig. 3 that the amplitude ratio derived from the approximate expression Eq. (2.17) is nearly identical to the exact derivation Eq. (2.32). Thus, it appears that the conservation of heat flux at the interface between the small and large wires of the schematic of fig. 1 is of secondary importance.

Also included in fig. (3) are the numerical computations of Stocks (1986). These solutions represent explicit finite difference solutions to the one dimensional unsteady heat transfer equation as shown in Eq. (2.1). The small deviation of the numerical results from the exact solution at low frequency in fig. (3) is apparently due to the unsteady character of the numerical results. Similar computations of the phase angle Φ for the type B thermocouple are represented in fig. 4. As indicated, the phase angle varies over the range $0 \geq \Phi \geq -\pi/2$ and approaches the lower limit of $-\pi/2$ for large frequencies $\omega/\omega_n \gg 1$.

The spacial variation of the amplitude ratio $|T(x)|$ derived from Eqs. (2.17) and (2.32) is graphed in fig. 5. These computations were made at an angular frequency of $\omega/\omega_n = 0.1$ for the type B thermocouple. As evident in fig. 5, the difference between the exact and approximate expression is somewhat exaggerated at a very low frequency. Nevertheless, the error represented by the approximate solution is less than 7% over the length of the thermocouple. As stated earlier, matching the heat flux at the interface between the small and large wire at $x = \pm l$ in the schematic of fig. 1 appears to be of secondary importance in relation to providing a

the two material approximate solution Eq. (2.40) and the values of the boundary conditions for T_a and T_b substituted from Eqs (2.38) and (2.39). The same conclusion can be drawn with respect to the phase angle Φ , shown in fig. 10.

The spacial variation of the amplitude ratio $|T(x)|$ derived from Eqs. (2.17) and (2.40) is plotted in fig. 11. These computations were made at an angular frequency of $\omega/\omega_n = 0.1$ for the type B thermocouple with the dimensions listed in table 2. It is interesting to note the small asymmetry in the amplitude ratio on the left and right side of the junction. This asymmetry is the result of the small differences in the physical properties across the junction as listed in table 2.

The steady state amplitude ratio $|T(0)|$ for a type T thermocouple is plotted in fig. 12 using equations (2.17) and (2.40). The dimensions and material properties are listed in table 2. The average material properties listed in Table 2 were used to compute the amplitude ratio of the frequency response with the one material solution, Eq. (2.17). Also plotted in fig. 12 is the amplitude ratio derived from the two material solution, Eq. (2.40). In the latter case, the individual material properties also listed in table 2 were used.

As indicated in fig. 12, the amplitude ratio for the approximate one material steady-state frequency response of a type T thermocouple is distinctly different from the two material approximate solution. This is a consequence of unequal material properties across the junction for the type T thermocouple. Also shown in fig. 12 is a numerical solution of the second order ordinary differential equation for the temperature, Eq. (2.6). The numerical finite difference solution of the boundary value problem of Eq. (2.6) matches both the temperature and heat flux at

measured for a range of frequencies.

2.5.1 Rotating Wheel Experiment

A rotating wheel configuration was used to deliver the test airstream to the proposed sensors. A similar experimental apparatus is described in detail by Elmore et al. (1986). A schematic of the rotating wheel apparatus used in the present experiment is shown in figure 15. As the wheel rotates, the holes pass the two air supply tubes which allow slugs of hot and cold air to alternately enter a transition tube assembly mounted directly above the rotating wheel. In the transition tube the slugs of hot and cold air coalesce into a single air stream providing roughly a square wave temperature profile covering a range of frequencies from roughly 1 to 30 Hz.

The analog temperature signal was digitized with a Data Translation DT-2801 board mounted in an expansion slot of an IBM AT compatible computer as shown in figure 15. The ASYST software loaded on the hard disc of the personal computer provided a flexible system for data storage, manipulation and display.

The true temperature profile of the airstream was measured with a constant current anemometer (TSI 1054-A) and sensor (1226 PI 2.5).

2.5.2 Thermocouple Construction

Thermocouple wire of the desired length and type is threaded into the four hole ceramic with the thermocouple end last. Three or four kinks are made in each wire near the thermocouple end so the wire must be firmly pulled into the tube leaving enough wire sticking out to make the thermocouple. Drops of epoxy

two channels at a sampling rate of 512 Hz per channel for a total sample time of two seconds. The ASYST software code is listed in figure 17.

The ASYST code first plotted the temperature profiles versus time from the thermocouple and anemometer and an example of the plot is shown in figure 18. The ASYST software next took the Fast Fourier Transform of the temperature data in each channel and recorded the amplitude ratio and phase angle between both channels at the first harmonic for the square wave. These data are discussed in the next section.

2.6 EXPERIMENTAL RESULTS

Initial tests with a signal generator and the output from an RC circuit indicated that the ASYST code and data acquisition hardware were operating properly. Several test sensors were constructed and tested with the dimensions listed in table 3. In each case measurements of the amplitude and phase angle were compared with the appropriate theory. A discussion of the results is given below.

2.6.1 First Order Response

The amplitude ratio and phase angle were measured with the type K thermocouple listed first in table 3. The lengths of the thermocouple and support wires in this case were chosen to eliminate the effects of axial heat conduction. The experimental data representing the amplitude ratio are plotted in figure 19 along with the theory representing a first order frequency response. The experimental data were correlated with a natural frequency $\omega_1 = 5.5 \text{ sec}^{-1}$ and a

the data and theory were correlated by assuming that the material properties are uniform across the thermocouple junction. In this case the data were correlated with a natural frequency $\omega_1 = 5.0 \text{ sec}^{-1}$ and a thermal diffusivity of $\alpha = .059 \text{ cm}^2 / \text{sec}$.

As indicated in figure 21 the data has been correlated with the theory to within 10% over most of the range of wheel frequencies. The data is reproducible but again a noticeable drift of the experimental data exists relative to the theory as was discussed in the previous section.

Also plotted in figure 22 are experimental data representing the phase angle Φ for the frequency response of the shortened type K thermocouple. The data is correlated to within 7% of the theory. The experimental data for the phase angle also indicate a small drift in the natural frequency ω_1 .

T	=	steady-state frequency response
T_f	=	amplitude of periodic gas temperature ($^{\circ}K$)
T_g	=	gas temperature ($^{\circ}K$)
T_0	=	mean gas temperature ($^{\circ}K$)
\vec{T}_w	=	complex amplitude of periodic wire temperature($^{\circ}K$)
T_w	=	local wire temperature ($^{\circ}K$)
v	=	gas velocity ($cm - s^{-1}$)
x	=	axial distance from center of wire (cm)

Greek Symbols

α	=	thermal diffusivity ($cm^2 - s^{-1}$)
γ	=	α / ω_n (cm^2)
ν_f	=	kinematic viscosity of gas ($cm^2 - s^{-1}$)
ω	=	angular frequency (s^{-1})
ω_n	=	natural frequency of wire ($= 4h / \rho c D$)(s^{-1})
Φ	=	phase angle
ρ	=	material density (gm - cm ⁻³)
Δ_1	=	dimensionless function
Δ_2	=	dimensionless function

2.9 TABLES AND FIGURES

Table 1 - Properties of One Material Wire (Type B)

Dimensions (cm)

$\underline{D_1}$	$\underline{D_2}$	$\underline{D_2/D_1}$	\underline{l}	\underline{L}
.025	.05	2	.2	.35
.0076*	.038	5	.1	.2

Average Properties of Type B

$\rho c \left(\frac{J}{cm^3 - ^\circ K} \right)$	$\alpha \left(\frac{cm^2}{sec} \right)$
3.8	.22

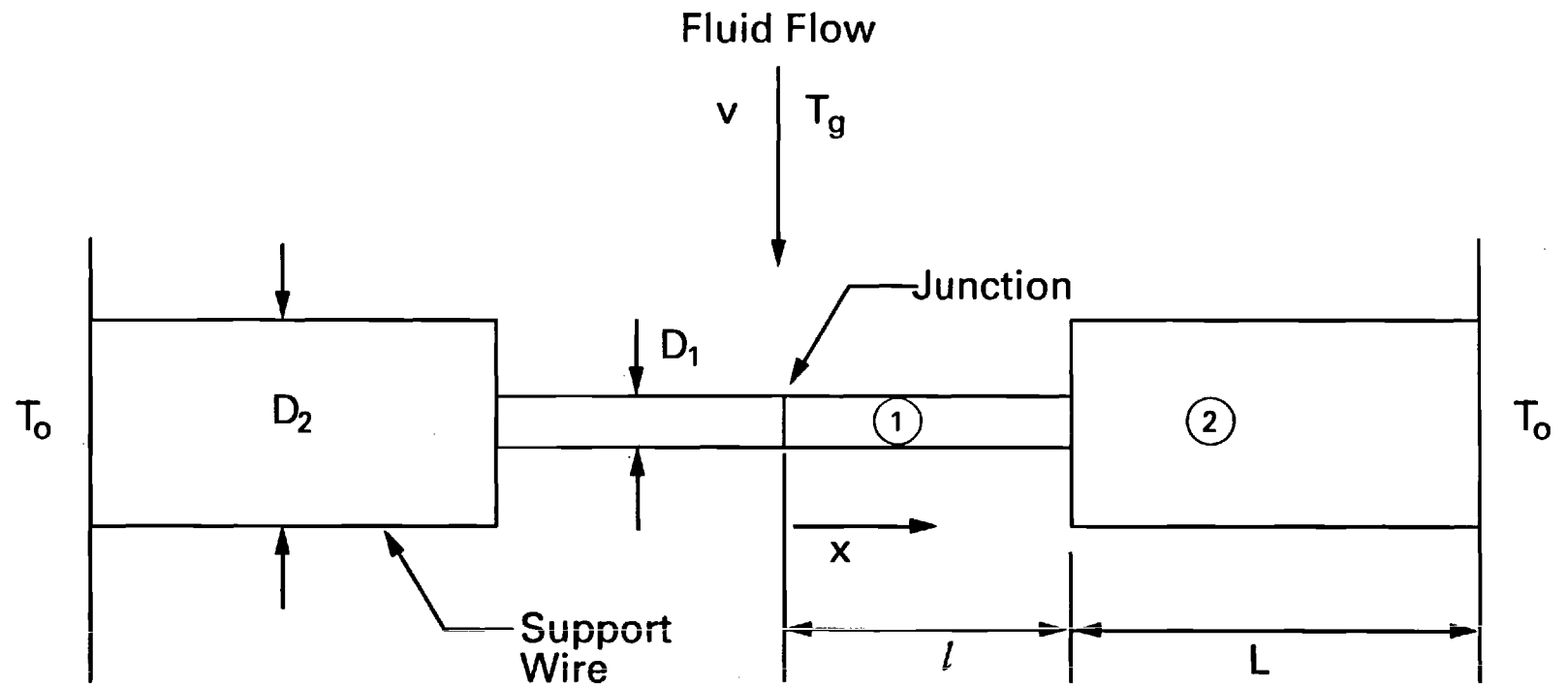
Gas Properties

$$T_0 = 900^\circ K$$

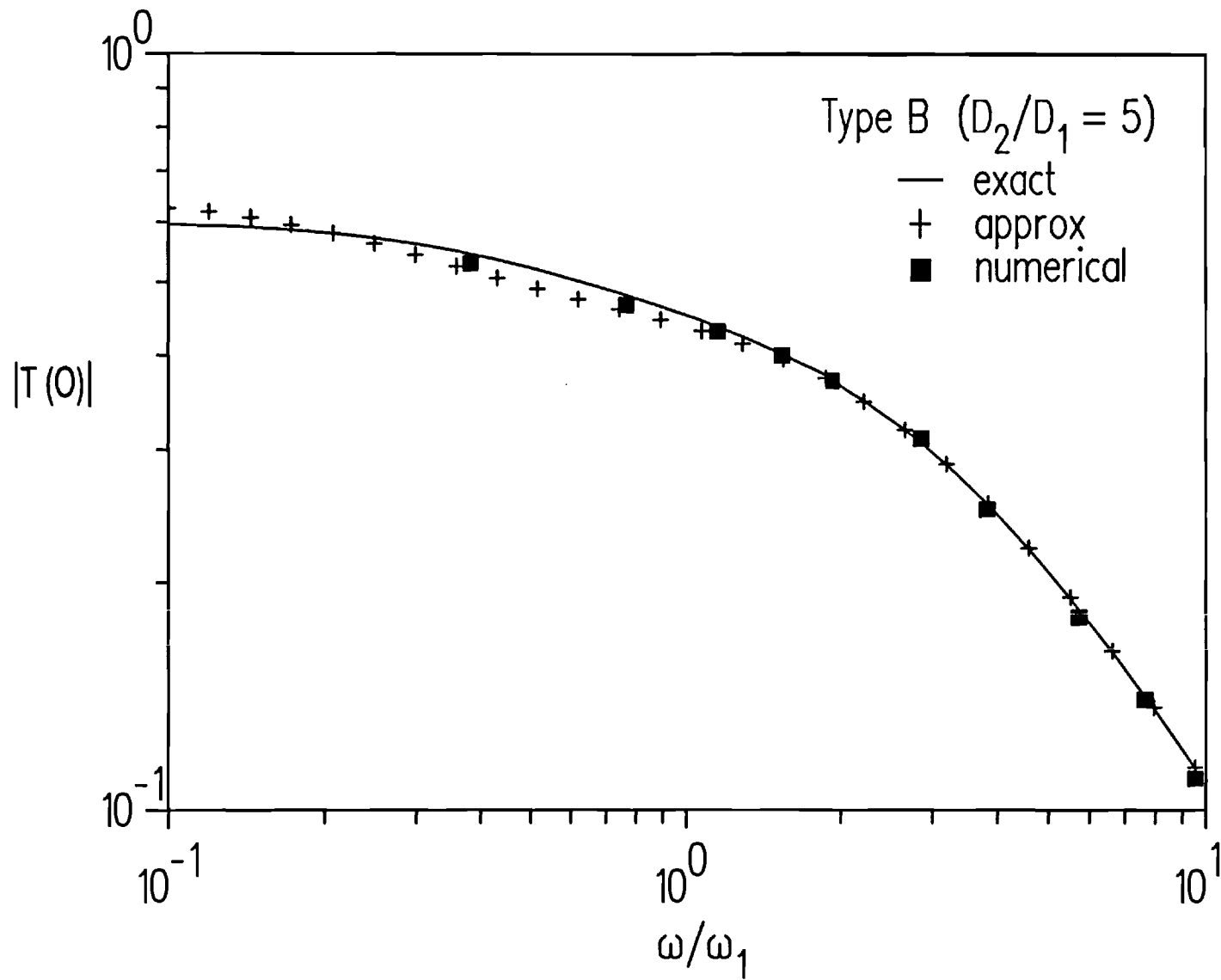
$$M = .26$$

$$P = 1 \text{ atm}$$

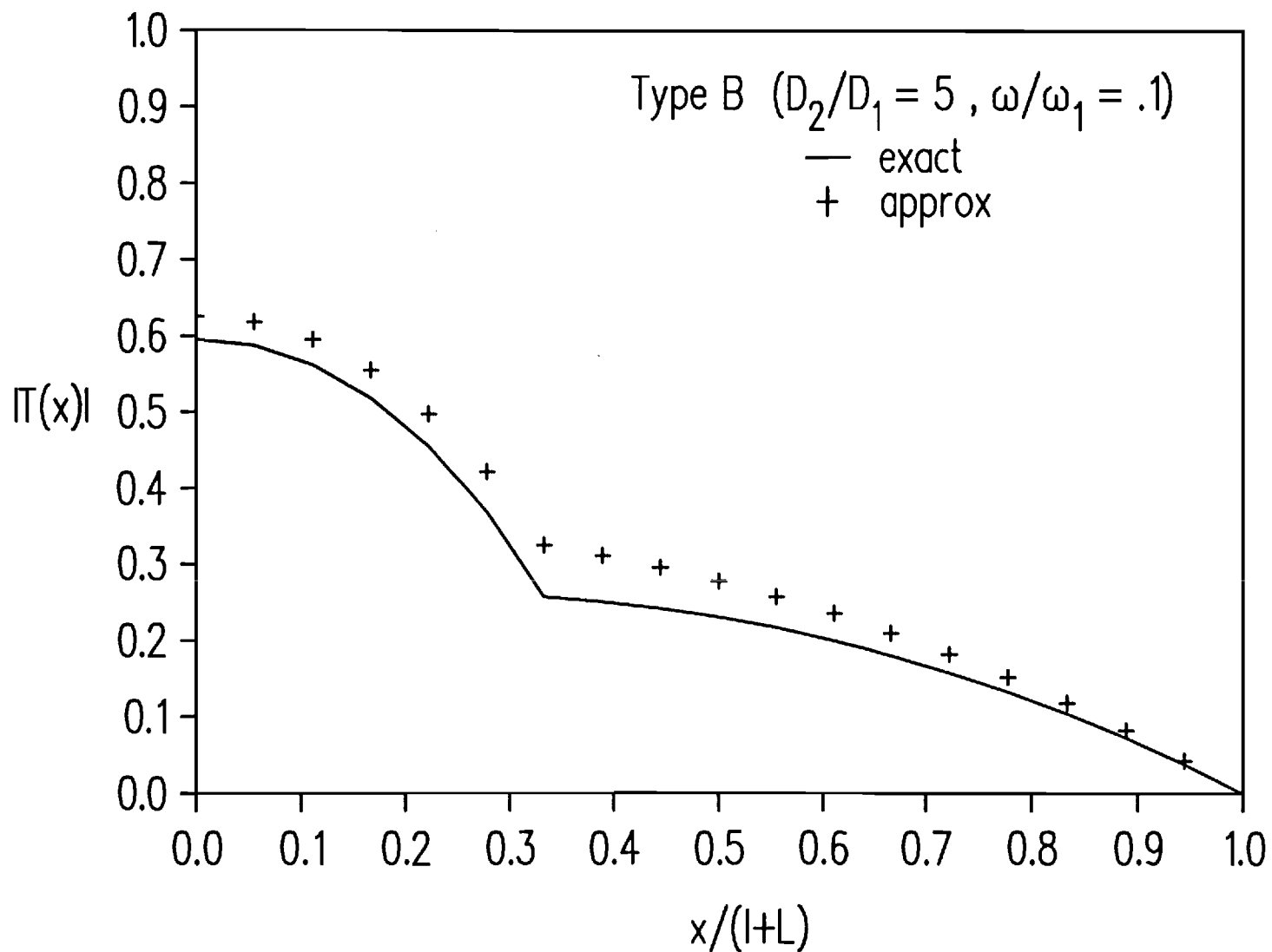
$$*\omega_1 = 32.9 \text{ sec}^{-1}$$



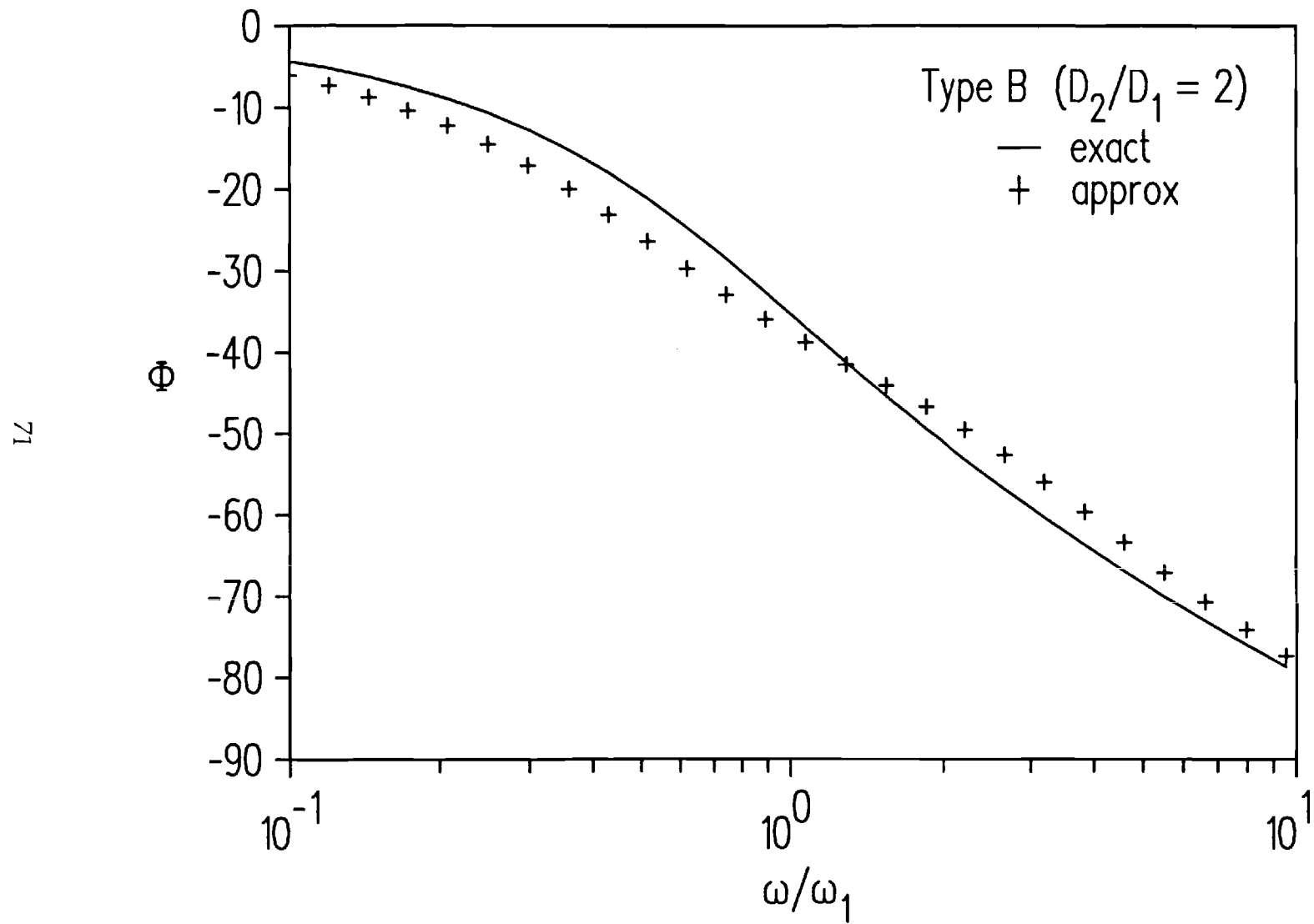
1. Schematic of one material supported wire.



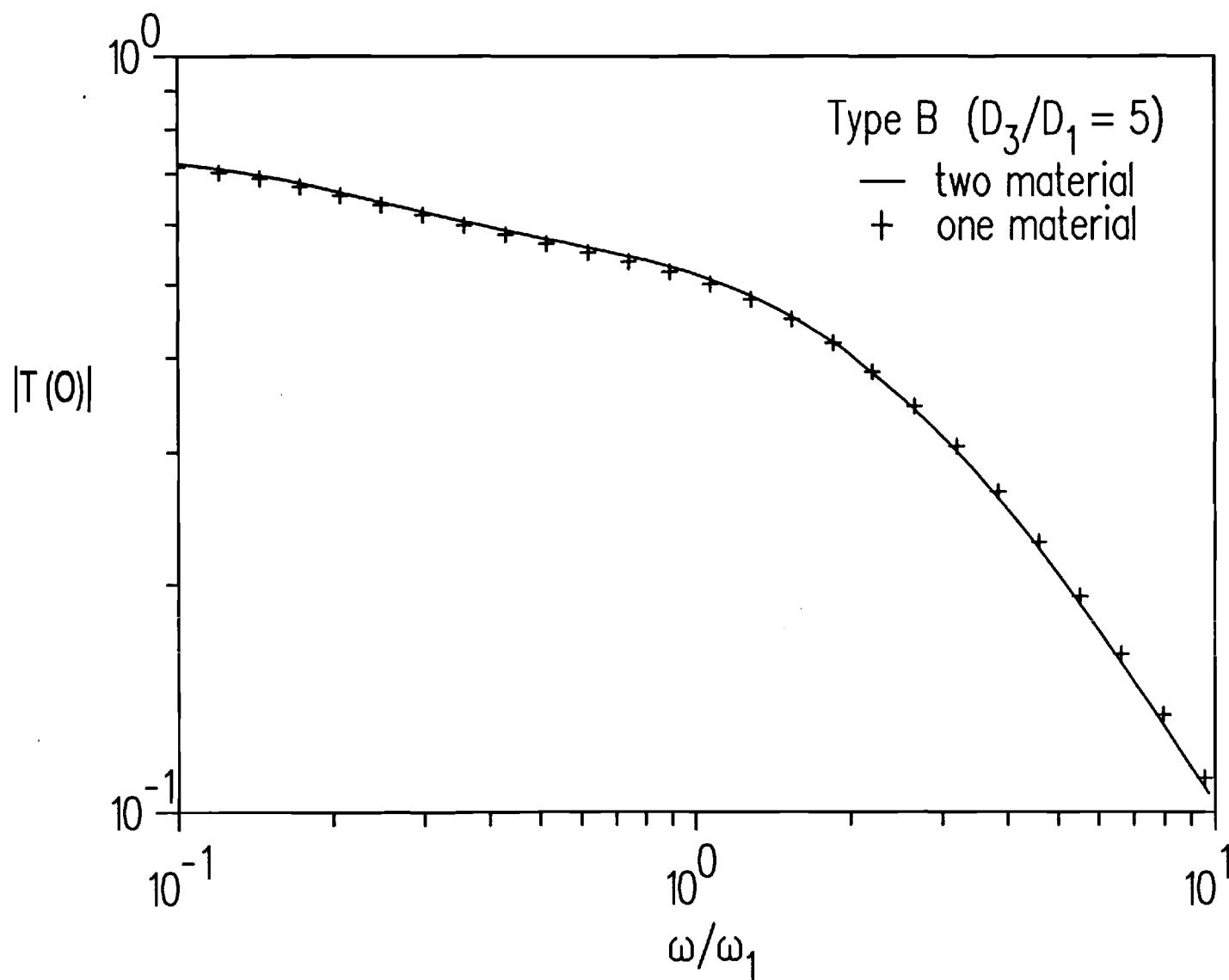
3. Amplitude ratio vs. angular frequency for one material wire. Solid line is exact solution Eq. (32); Crosses are approximate solution Eq. (17).



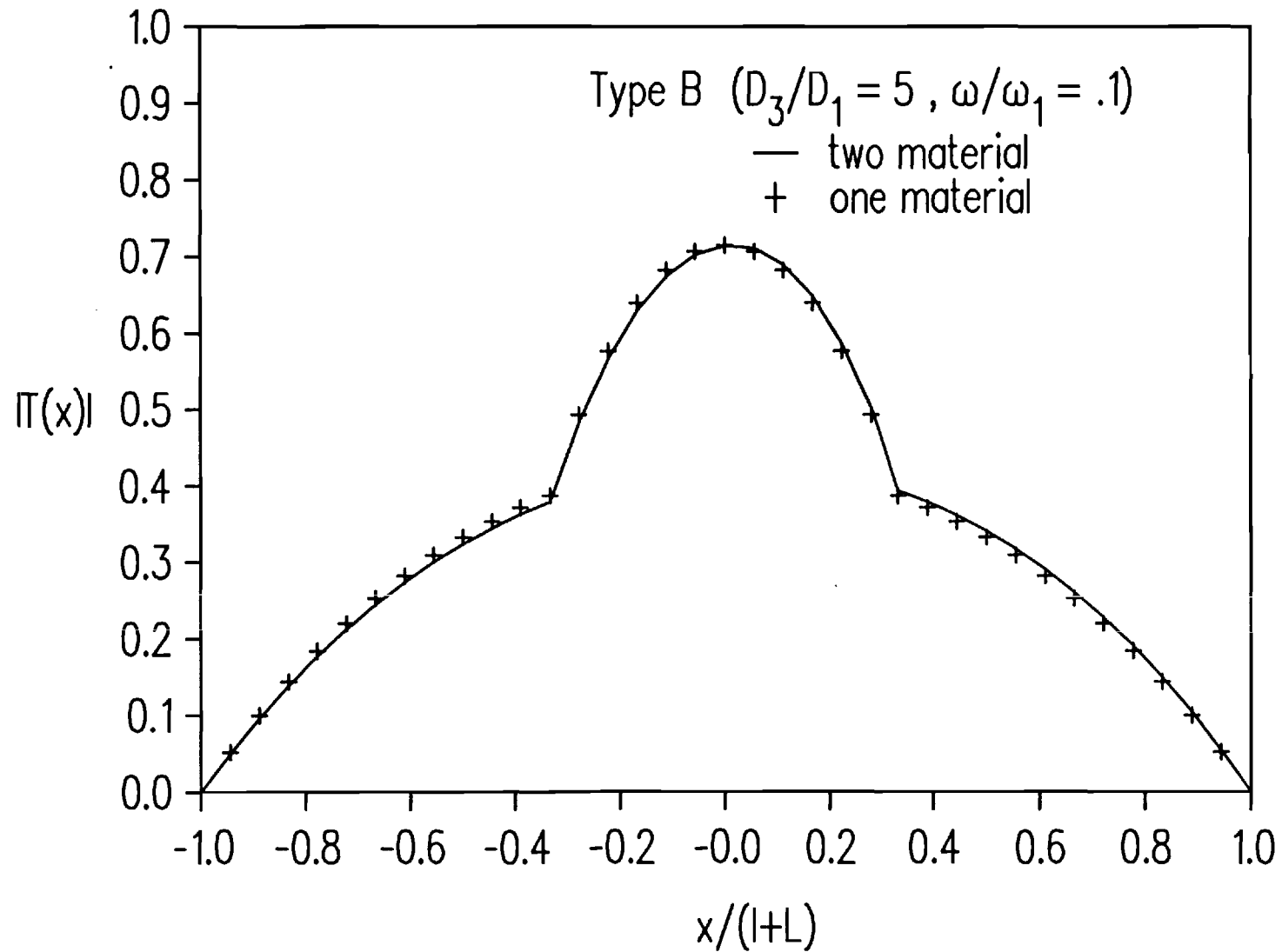
5. Amplitude ratio vs. distance for one material wire. Solid line is derived from Eqs. (24) and (31). Crosses are derived from Eqs. (14) and (16).



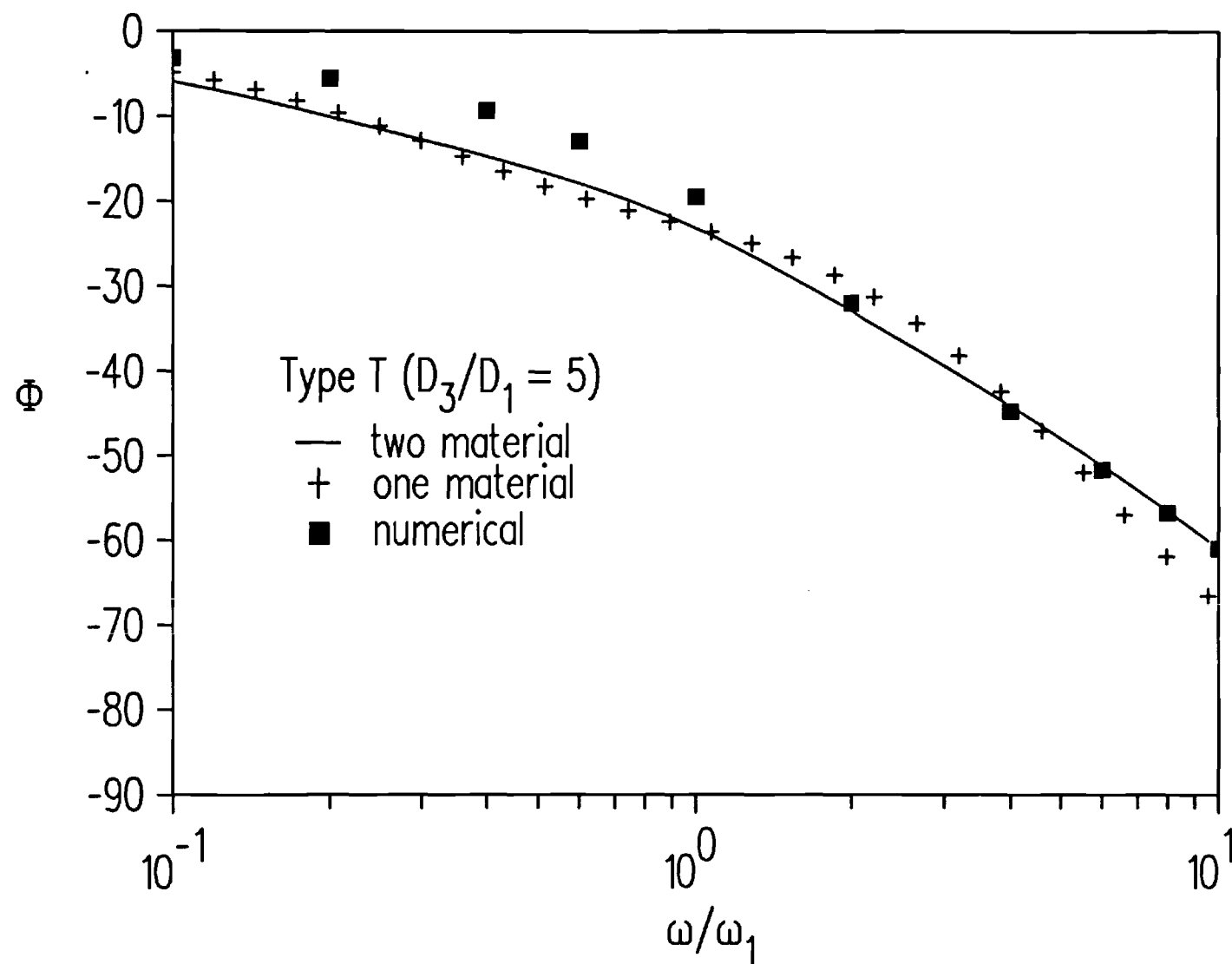
7. Phase angle vs. angular frequency for one material wire. Solid line is Eq. (32). Crosses are Eq. (17).



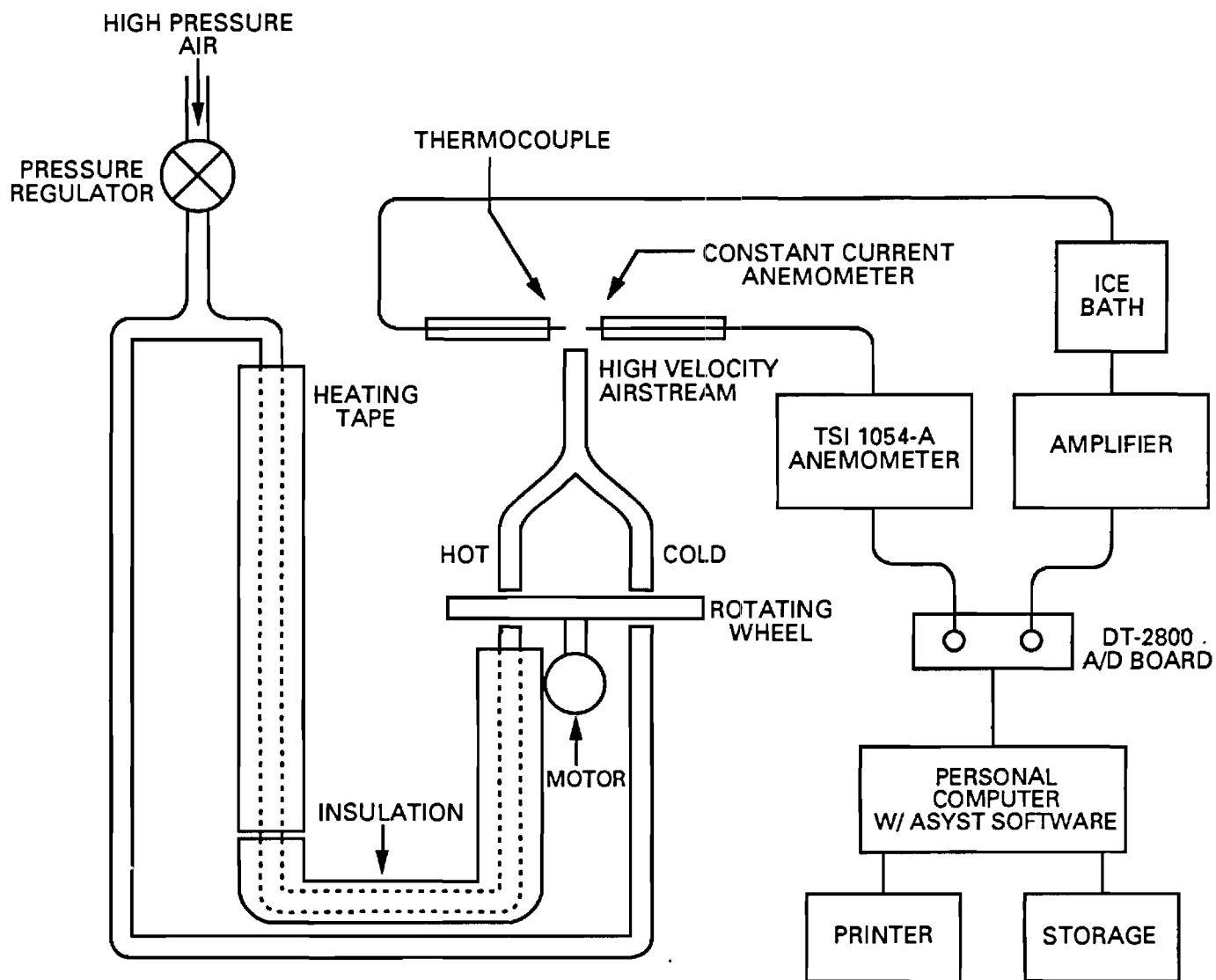
9. Amplitude ratio vs. angular frequency for two material wire. Solid line is Eq. (40). Crosses are approximate one material solution Eq. (17).



11. Amplitude ratio vs. distance for two material wire. Solid line derived from Eqs. (36a) and (36b). Crosses are approximate one material solution Eqs. (14) and (16).



13. Phase angle vs. angular frequency for two material wire. Solid line is Eq. (40). Crosses are approximate on material solution Eq. (17).



15. Rotating wheel experiment.

```

FORGET.ALL
REAL DIM[ 1024 ] ARRAY TIME
COMPLEX DIM[ 1024 ] ARRAY TRANS
REAL DIM[ 6 ] ARRAY ANS
REAL DIM[ 1024 ] ARRAY ZMAGO
REAL DIM[ 1024 ] ARRAY ZARGO
INTEGER SCALAR NUM
REAL SCALAR MEN
REAL SCALAR CD
REAL DIM[ 1024 ] ARRAY FREQS
REAL DIM[ 1024 ] ARRAY SIGNAL
INTEGER      dim[ 1024 , 2 ] array DATA.BUFFER

```

```

1. CD :=
.0000 DATA.BUFFER :=
LOAD.OVERLAY ACQUIS.SOV
.0000 1.0000 A/D.TEMPLATE DEMO.TEMPLATE \ DEFINE AN A/D TEMPLATE
DATA.BUFFER TEMPLATE.BUFFER           \ DECLARE ARRAY AS A TEMPLATE BUFFER
CYCLIC                                \ SET TEMPLATE BUFFER TO CYCLIC MODE
2048.0000 TEMPLATE.REPEAT              \ SET REPETITIONS FOR I/O INSTRUCTION
CD CONVERSION.DELAY                    \ CONVERSION RATE (MSECS/SAMPLE)
DEMO.TEMPLATE A/D.INIT                  \ INITIALIZE CURRENT A/D TEMPLATE
A/D.IN>ARRAY                            \ A/D INPUT TO TEMPLATES BUFFER
LOAD.OVERLAY WAVEOPS.SOV
1024 REAL RAMP 1 - 2 * CD * 1000 / TIME := \ SET TIME AXIS

DATA.BUFFER XSECT[ 1 ] 2048 -           \ CHANNEL 1 ON STACK (ANEMOMETER)
SIGNAL := SIGNAL
-2048 / 10 * -55.274 * 353. +           \ CALIBRATE (DEGREES C)
SIGNAL := SIGNAL
0.5 SET.CUTOFF.FREQ                     \ SMOOTH DATA (CYCLES/POINT)
SMOOTH SIGNAL := SIGNAL
MEAN MEN := SIGNAL
MEN - SIGNAL :=                         \ CENTER ON ORIGIN
TIME SUB[ 1 , 500 , 1 ] SIGNAL SUB[ 1 , 500 , 1 ]
XY.AUTO.PLOT SIGNAL                     \ PLOT CHANNEL 1
FFT                                     \ TAKE FFT
TRANS := TRANS ZMAG ZMAGO :=           \ MAGNITUDE OF FFT
5 SET.#.POINTS
1 SET.#.OPTIMA
ZMAGO SUB[ 1 , 120 , 1 ] LOCAL.MAXIMA \ FIND INDEX AND MAX OF MAGNITUDE
SWAP NUM := NUM                         \ INDEX OF MAX MAGNITUDE
1 - CD / 1024. / 1000 * PI *           \ FREQUENCY AT MAX MAGNITUDE
ANS [ 1 ] := ANS [ 1 ] DROP ANS [ 2 ] :=
TRANS [ NUM ] DEG ZARG ANS [ 3 ] :=    \ ARGUMENT AT MAX MAGNITUDE

```

```

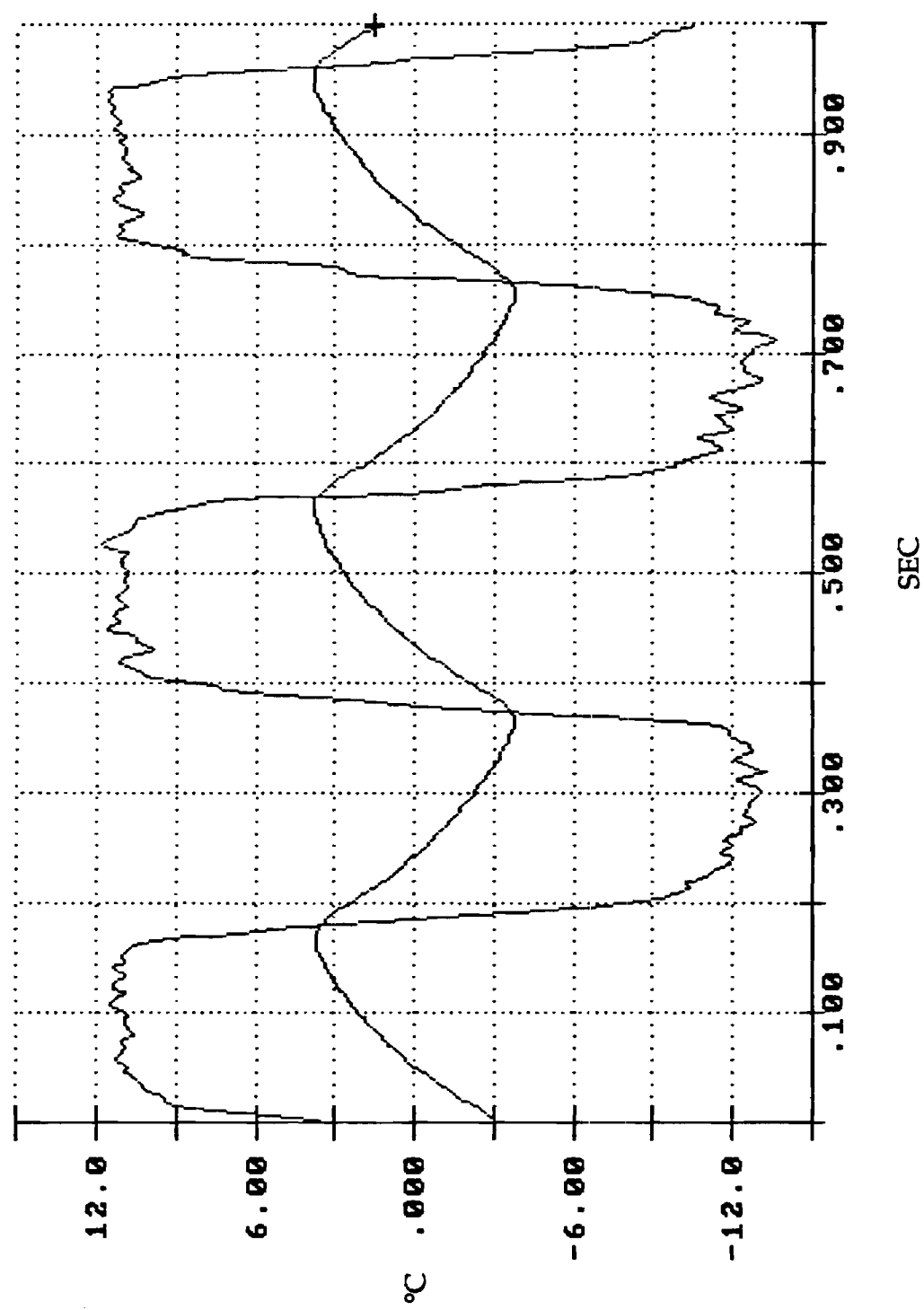
DATA.BUFFER XSECT[ 2 ] 2048 -           \ CHANNEL 2 ON STACK (THERMOCOUPLE)
SIGNAL := SIGNAL
.124 * SIGNAL := SIGNAL                 \ CALIBRATE (DEGREES F)
0.5 SET.CUTOFF.FREQ                     \ SMOOTH DATA (CYCLES/POINT)
SMOOTH SIGNAL := SIGNAL
MEAN MEN := SIGNAL

```

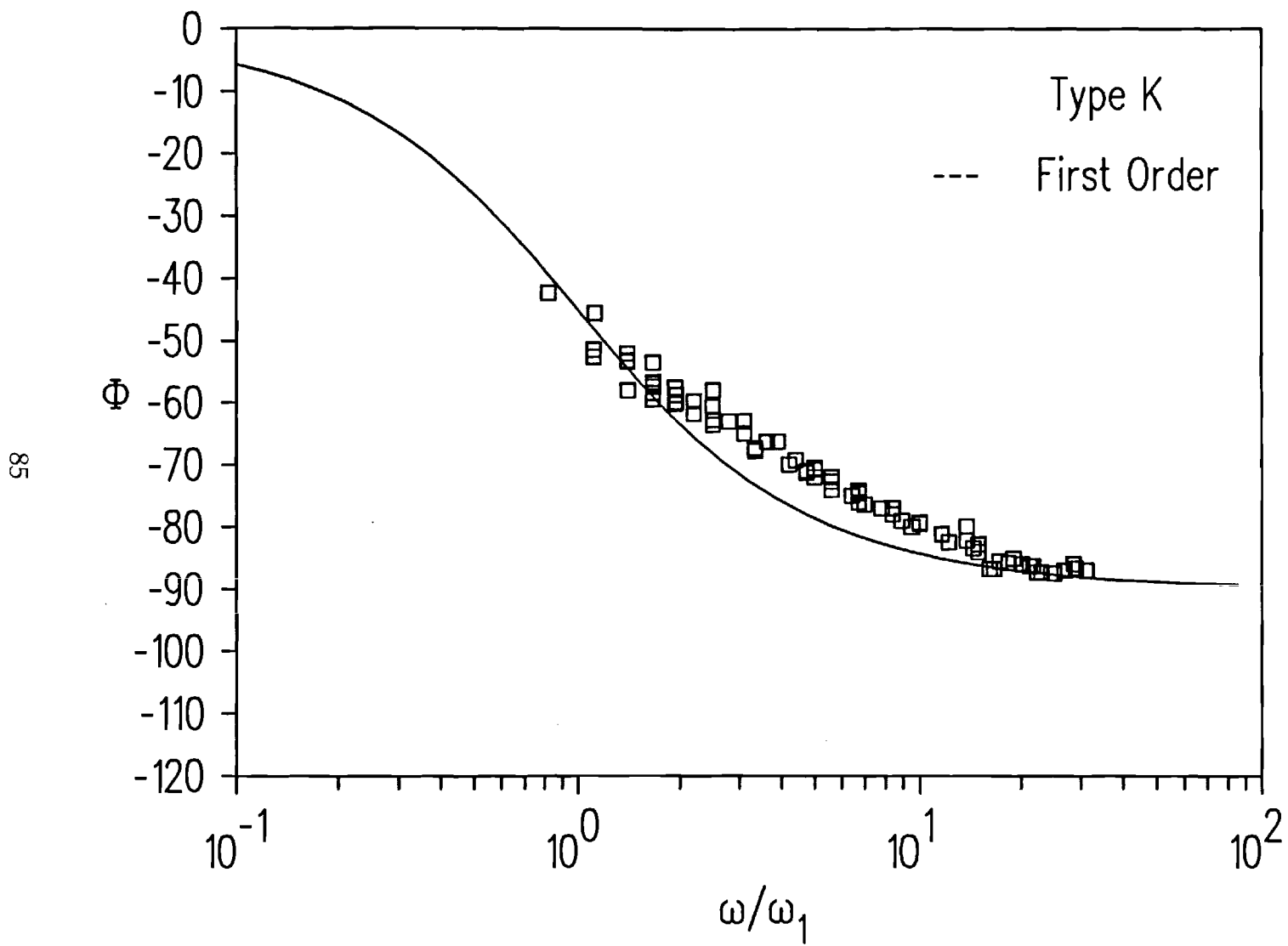
```

ASYST Version 3.00
Page 1      TEMP3.FOR    03/13/91    11:42:33.77

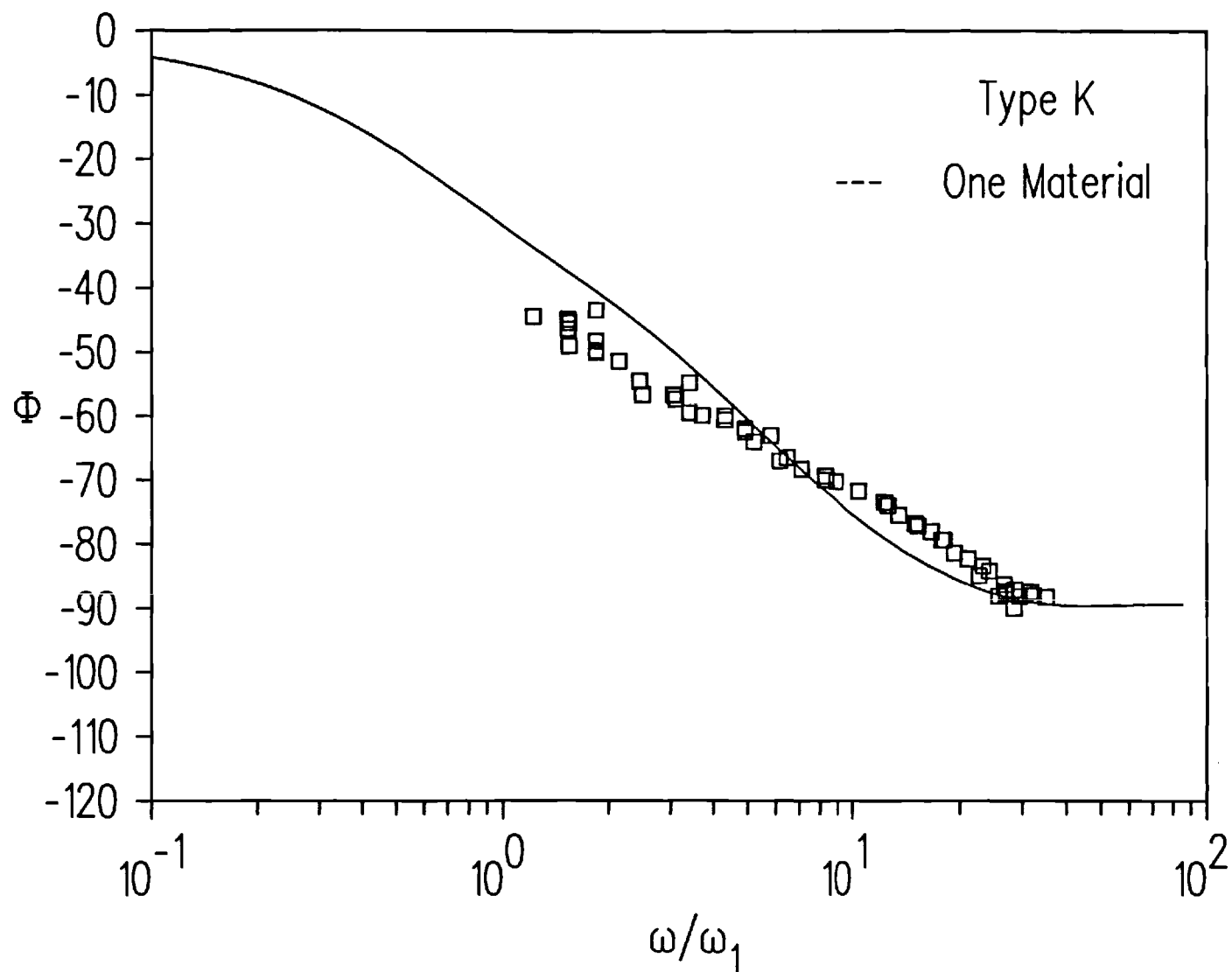
```



18. Gas Temperature Profile



20. Phase angle vs. angular frequency. $\omega_1 = 5.5 \text{ sec}^{-1}$, $\alpha = .059 \text{ cm}^2 / \text{sec}$.



22. Phase angle vs. angular frequency. Solid line is derived from Eq. (32).
 $\omega_1 = 5.0 \text{ sec}^{-1}$, $\alpha = .059 \text{ cm}^2 / \text{sec}$.

3.0 MEASUREMENT OF FREQUENCY RESPONSE

Experimental measurements are made for the steady-state frequency response of a supported thermocouple wire. In particular, the effects of axial heat conduction are demonstrated for both a supported one material wire (type K) and a two material wire (type T) with unequal material properties across the junction. The data for the amplitude ratio and phase angle are correlated to within 10% with the theoretical predictions of Forney and Fralick (1991). This is accomplished by choosing a natural frequency ω_n for the wire data to correlate the first order response at large gas temperature frequencies. It is found that a large bead size, however, will increase the amplitude ratio at low frequencies but decrease the natural frequency of the wire. The phase angle data are also distorted for imperfect junctions.

3.1 INTRODUCTION

The evaluation of jet engine performance and fundamental studies of combustion phenomena depend on the measurement of turbulent fluctuating temperatures of the gas within the engine (Dils and Follansbee, 1976). Historically, these temperatures have been measured with thermocouples. The advantages of thermocouples are their low cost, reliability and simplicity since they do not require optical access or elaborate support electronics. However, the design of a thermocouple represents a compromise between accuracy, ruggedness and rapidity of response.

thermocouple is normally constructed manually, there are a number of physical imperfections that can affect the response. For example, three joints must be fabricated consisting of the thermocouple junction and joints at both ends of the thermocouple element. These three joints (welded or soldered) and the epoxy used to secure the support legs in the ceramic stick are darkened in the schematic at the bottom of figure 1. As indicated in figure 1, the supported thermocouple may not be symmetrical and there may be additional material or beads at the joint locations.

3.2.1. Physical Dimensions

The thermocouple support wires and the smaller thermocouple elements were analyzed by Elmore et al. (1983) for stresses at the maximum flow conditions for the F100 gas turbine engines of $T = 1680^{\circ}\text{K}$, $P = 2.01 \times 10^6 \text{ Newton/meter}^2$ (202 psia) and a gas Mach number $M = 0.36$. The sensor location for these calculations corresponded to a wall position between the vanes downstream of the combustor exit. Elmore et al. (1983) also assumed an allowable stress in the thermocouple wire of $4.39 \times 10^7 \text{ Newton/meter}^2$ (6360 psi). The maximum allowable length-to-diameter ratio L/D for the support wire was thus calculated to be 6.5 while the maximum value for the thermocouple element was found to be 15.5.

Elmore et al. (1986) also limited the smallest diameter of the thermocouple wire to $76 \mu\text{m}$ (.003 in) because of limitations to junction fabrication. These constraints limit the length of the thermocouple element on each side of the junction to roughly 1 mm or to a total length of 2 mm for the thermocouple wire

however, there are four natural frequencies. For example, two of these frequencies are $\omega_1 = 4h_1/\rho_1 c_1 D_1$ and $\omega_2 = 4h_1/\rho_2 c_2 D_1$ on both sides of the junction.

3.2.3 Construction

Thermocouple wire of the desired length and type was threaded into the ceramic with the thermocouple end last. Three or four kinks were made in each wire near the thermocouple end so the wire must be firmly pulled into the tube leaving enough wire sticking out to make the thermocouple. Drops of epoxy were picked up with a piece of .010 in. diameter wire, added to the ceramic tube at A (see fig. 3) and pushed down around both wires. The kinks and epoxy firmly fasten the wires in the ceramic so they do not twist when the free ends are manipulated for electrical connections.

The junction at B in fig. 3 was made by cutting the large wire about half way through with a razor blade, laying the small diameter wire in the cut, and silver soldering the cut closed. After the solder, the excess wire ends that protrude through the soldered area were bent and broken off to clean up the junction.

The type T thermocouple junctions at C in fig. 3 were constructed successfully by one of two procedures. In the first procedure, the silver solder wire was coated with flux and the end heated with a torch until a drop formed. A twisted pair of thermocouple wires was pushed briefly into the flux coated solder drop. The solder wetted the pair up to where the twist stops. Using a razor blade and tweezers under a microscope, the thermocouple was bent and trimmed until collinear. The silver solder technique was also used to fabricate the chromel alumel (type K)

of varying frequency. A rotating wheel configuration is used to deliver the test air stream to the proposed sensors. A similar experimental apparatus was described in detail by Elmore et al. (1986).

A schematic of the rotating wheel apparatus used in the present experiment is shown in fig. 5. As the wheel rotates, holes pass the two air supply tubes (3/4 in. ID copper) that allow slugs of hot ($\leq 55^{\circ}\text{C}$) and cold ($\sim 30^{\circ}\text{C}$) air to alternately enter a transition tube assembly mounted directly above the rotating wheel. In the transition tube the slugs of hot and cold air coalesce into a single air stream providing roughly a square wave temperature profile covering a range of gas temperature frequencies from roughly 1 to 30 Hz. A 3/4 in. to 1/2 in. smooth copper adaptor was inserted at the end of the coalescing tube (location of thermocouple) in fig. 5 to increase the air velocity to 18 m/sec.

The analog temperature signal is digitized with a Data Translation DT-2801 A/D board mounted in an expansion slot of an IBM AT compatible computer as shown in fig. 5. ASYST software was loaded onto the hard disc of the personal computer and this provided a flexible system for data storage, manipulation and display. The true temperature profile of the airstream is measured with a constant current anemometer (TSI 1054-A) and sensor (1226 PI2.5).

3.4 EXPERIMENTAL PROCEDURE

3.4.1 Calibration

The air velocity at the exit of the coalescing tube in fig. 5 (location of thermocouple) was maintained at roughly 17.5 to 18 m/sec. The voltage regulator

two channels at a sampling rate of 512 Hz per channel for a total sample time of two seconds. An example of the gas temperature profile for a square wave frequency of 2.5 Hz is illustrated in fig. 6 where the smooth profile is the thermocouple response. After data acquisition, the Fast Fourier Transform (FFT) is taken for each channel. The largest peak (first harmonic) in the amplitude of the FFT is located for each channel which provides the frequency of the temperature profile. The ASYST software also records the amplitude ratio and phase angle between both channels at the first harmonic. In the latter case, the software corrects the phase angle for the conversion delay between channels. The amplitude ratio and phase angle are recorded for each frequency setting of the rotating wheel.

3.4.3 Data Correlation

Once the amplitude ratio and phase angle are recorded for a large number of gas temperature frequencies ω for a given thermocouple, the amplitude ratio and phase angle are plotted on separate graphs. Both quantities are plotted as a function of the ratio of the angular frequency of the square wave temperature profile ω to the natural frequency ω_1 of the positive thermocouple element. The natural frequency $\omega_1 = 4h_1/\rho_1 C_1 D_1$ is chosen to fit the amplitude ratio at large frequencies since the amplitude ratio should coincide with the first order response (independent of axial heat conduction) at large ω .

The lengths of the thermocouple element l and support wire L are then chosen such that theoretical predictions of the amplitude ratio are correlated with the

$$T(0) = \frac{1}{\Delta_1} \left\{ Q_i \sinh q_2 l \left[T_a + \frac{1}{G_1} (\cosh q_1 l - 1) \right] + \sinh q_1 l \left[T_b + \frac{1}{G_2} (\cosh q_2 l - 1) \right] \right\} \quad (3.2)$$

where

$$Q_i = \frac{k_1 q_1}{k_2 q_2}$$

and

$$\Delta_1 = Q_i \cosh q_1 l \sinh q_2 l + \cosh q_2 l \sinh q_1 l .$$

The boundary temperatures T_a , T_b in Eq. (3.2) are given by the expressions

$$\begin{aligned} T_a = \frac{1}{G_3} + \left\{ \sinh q_3 L \left[\left(\frac{1}{G_4} - \frac{1}{G_3} \right) \cosh q_4 (l + L) - \frac{1}{G_4} \right] \right. \\ \left. - \frac{1}{G_3} [Q_s \cosh q_3 l \sinh q_4 (l + L) + \cosh q_4 (l + L) \sinh q_3 l] \right\} \left(\frac{1}{\Delta_2} \right) \end{aligned} \quad (3.3)$$

and

$$\begin{aligned} T_b = \frac{1}{G_4} + \left\{ Q_s \sinh q_4 L \left[\left(\frac{1}{G_3} - \frac{1}{G_4} \right) \cosh q_3 (l + L) - \frac{1}{G_3} \right] \right. \\ \left. - \frac{1}{G_4} [\cosh q_4 l \sinh q_3 (l + L) + Q_s \cosh q_3 (l + L) \sinh q_4 l] \right\} \left(\frac{1}{\Delta_2} \right) \end{aligned} \quad (3.4)$$

where

$$Q_s = \frac{k_1 q_3}{k_2 q_4}$$

$$\Delta_2 = Q_s \cosh q_3 (l + L) \sinh q_4 (l + L) + \cosh q_4 (l + L) \sinh q_3 (l + L)$$

Here, the wire elements 1 to 4 are shown in the schematic of a two-material thermocouple wire shown in figure 2.

Equation (3.2).

A value of the natural frequency $\omega_1 = 20 \text{ sec}^{-1}$ was chosen to correlate the data for the amplitude ratio at large frequencies $\omega/\omega_1 > 1$. As indicated in figure 8, the data for the amplitude ratio drift below the theoretical prediction by 10% for increasing gas temperature angular frequencies ω . Although the effect of axial heat conduction is properly accounted for in figure 8, the phase angle data also appear to be distorted and to lie significantly below the predictions. These effects are apparently due to the large bead diameter at the junction (greater than twice the diameter of the thermocouple wire). Here, as before, it was necessary to increase the wire length in Eq. (3.2) by 20% to correlate the data.

A type T thermocouple junction without a bead was constructed by laser heating with the support legs silver soldered, as before. The thermocouple had an element length of $l = 1.25 \text{ mm}$ and a support wire length of 2.5 mm . The thermocouple and support wires had diameters of $D_1 = 76 \text{ }\mu\text{m}$ and $D_2 = 380 \text{ }\mu\text{m}$, respectively. The amplitude ratio and phase angle were measured and the results were compared with theory.

A value of the natural frequency $\omega_1 = 28 \text{ sec}^{-1}$ was necessary to correlate the amplitude data at large frequencies. This represents a larger air velocity compared to the data in figure 8. As shown in figure 9, there appears to be less drift in the amplitude ratio below the theory compared to the previous results taken with a beaded junction. An improved correlation is also observed for the phase angle data plotted in figure 9. The predicted phase angle from Equation (3.2) correlates the data well and there appears to be less distortion of the phase angle data

and phase angle that reflect the effects of axial heat conduction are correlated to within 10% with the theoretical predictions of Forney and Fralick, (1991). To correlate the experimental data, it is necessary to choose a natural frequency ω_n (depends on gas properties and velocity) for the amplitude data at large gas temperature frequencies. If there is a bead at the junction (typically twice the wire diameter), it is necessary to increase the wire length l by 20% in the theory to correlate the data.

The use of silver solder for the junction and wire supports is adequate for both the type K and type T thermocouples but will leave a small bead. A spot welding procedure for the type K thermocouple, however, appears to introduce a large contact resistance since the measured amplitude ratio in this case was only a fraction of its predicted value. The use of laser heating to form the junction, however, left no bead and required no adjustments to the wire length in the theory to correlate the data. Moreover, the use of laser heating for the purpose of fabricating thermocouple junctions without beads appears to improve the correlation of both the amplitude ratio and phase angle data with theory. In particular, the phase angle data from a beadless junction exhibited far less distortion compared to theoretical predictions. Also, the wire lengths used in the theory to correlate the data were realistic for the laser heated junctions.

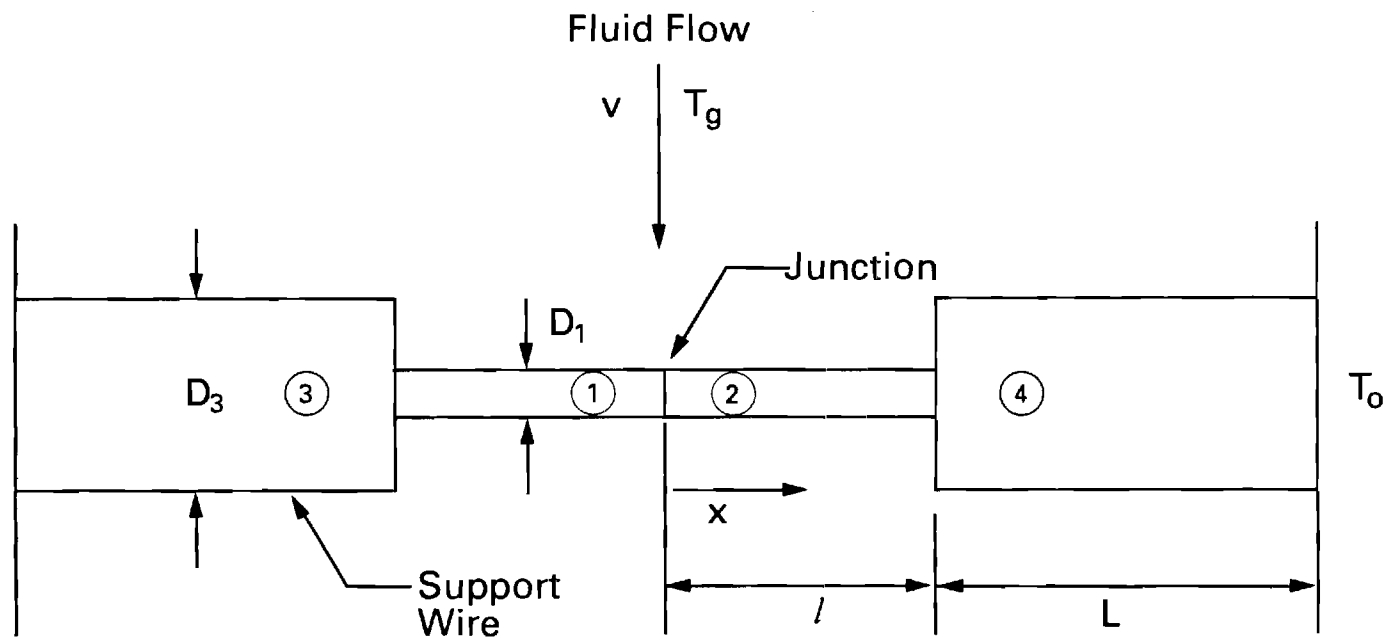
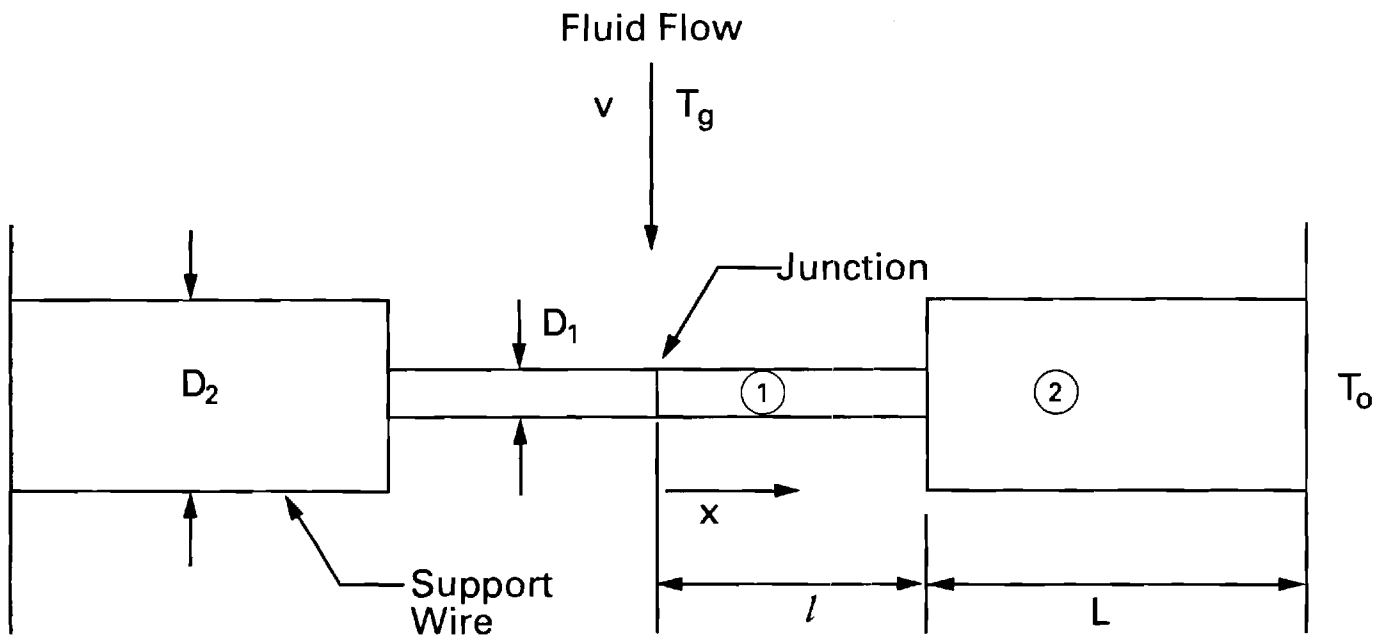
It is found that a large bead at the thermocouple junction increases the amplitude ratio at low frequencies but decreases the natural frequency of the wire. The phase angle data are also distorted for imperfect junctions.

ω_n	=	natural frequency of wire $(= 4h / \rho cD)(s^{-1})$
Φ	=	phase angle
ρ	=	material density (gm/cm^3)
Δ_1	=	dimensionless function
Δ_2	=	dimensionless function

3.9 TABLES AND FIGURES

Table 1 Properties of Thermocouples

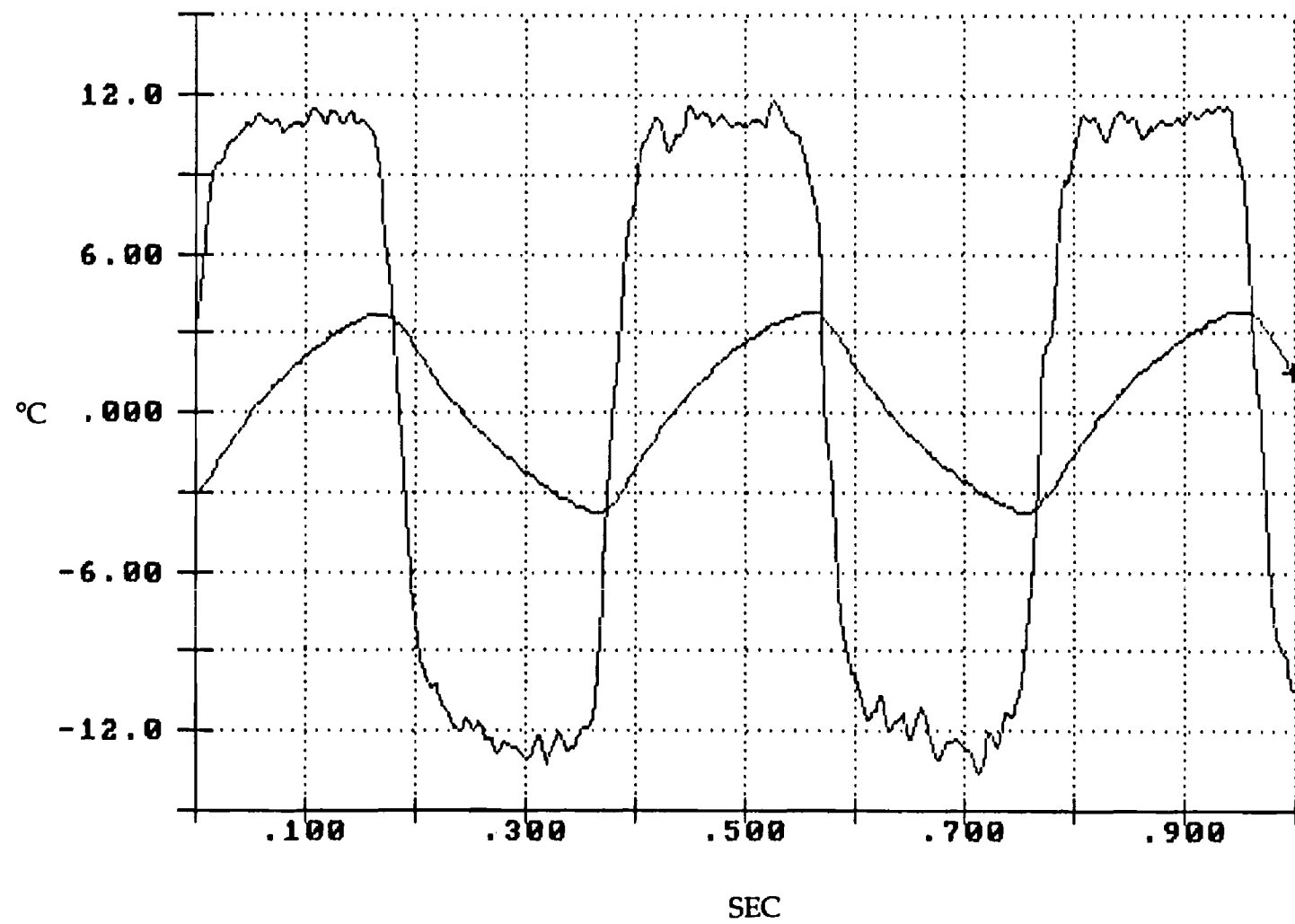
<u>Dimensions (cm)</u>				
<u>D₁</u>	<u>D₂</u>	<u>D₂/D₁</u>	<u>1</u>	<u>L</u>
.0076	.038	5	.1-.15	.17-.22
<u>Properties of Type K</u>				
	$\rho c \left[\frac{J}{cm^3 - ^\circ K} \right]$	$\alpha \left[\frac{cm^2}{sec} \right]$		
Chromel	3.80	.048		
Alumel	4.10	.070		
Average	3.95	.059		
<u>Properties of Type T</u>				
	$\rho c \left[\frac{J}{cm^3 - ^\circ K} \right]$	$\alpha \left[\frac{cm^2}{sec} \right]$		
Copper	3.44	1.16		
Constantan	3.48	.067		
Average	3.46	.614		
<u>Wire Location</u>				
<u>Region</u>	<u>Type K</u>	<u>Type T</u>		
left	Chromel	Copper		
right	Alumel	Constantan		



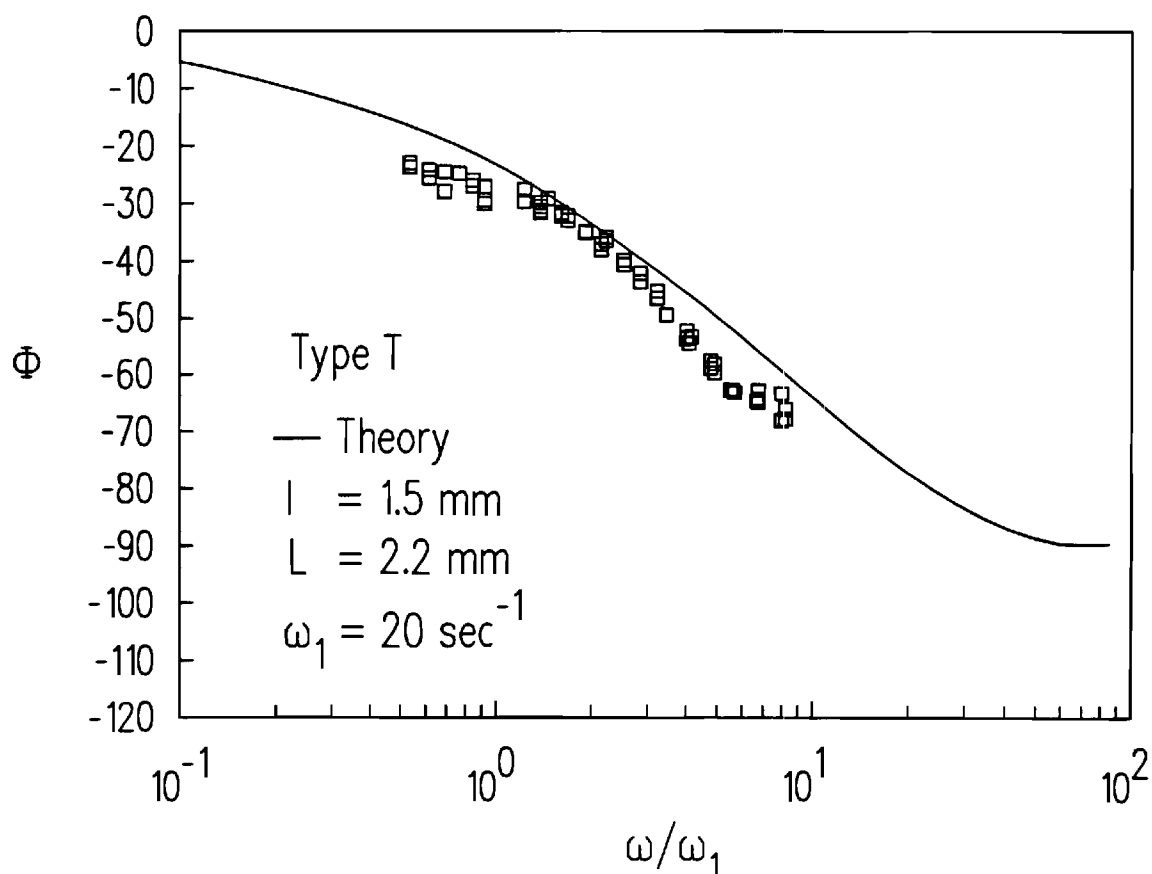
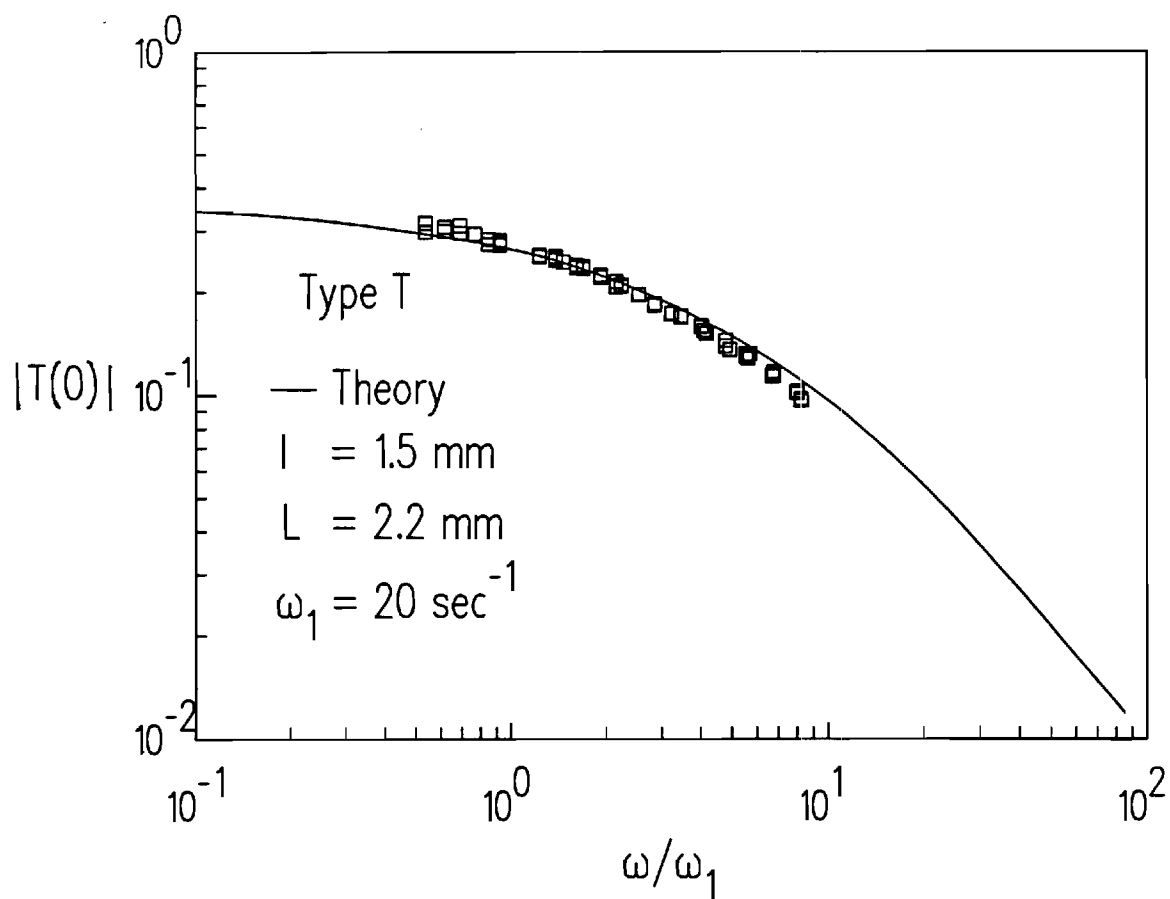
2. Schematic of One or Two Material Supported Wires



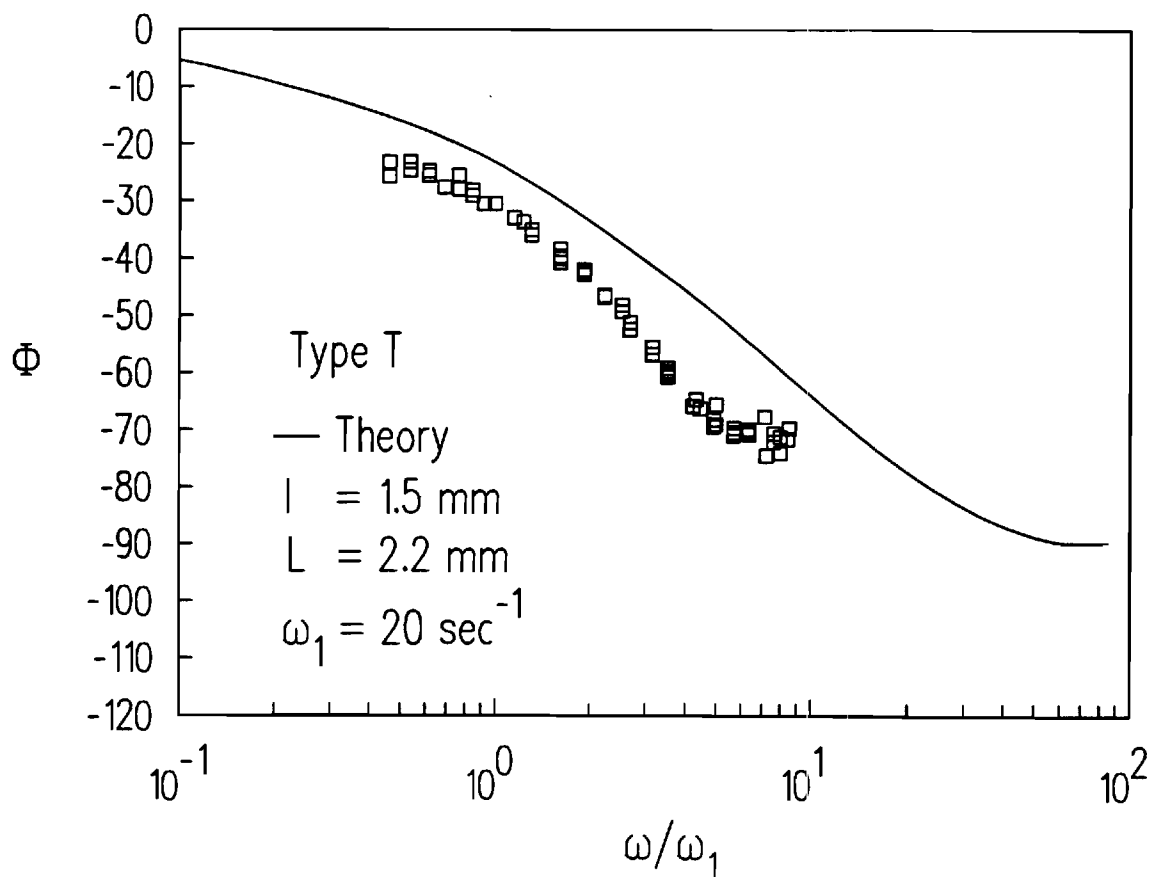
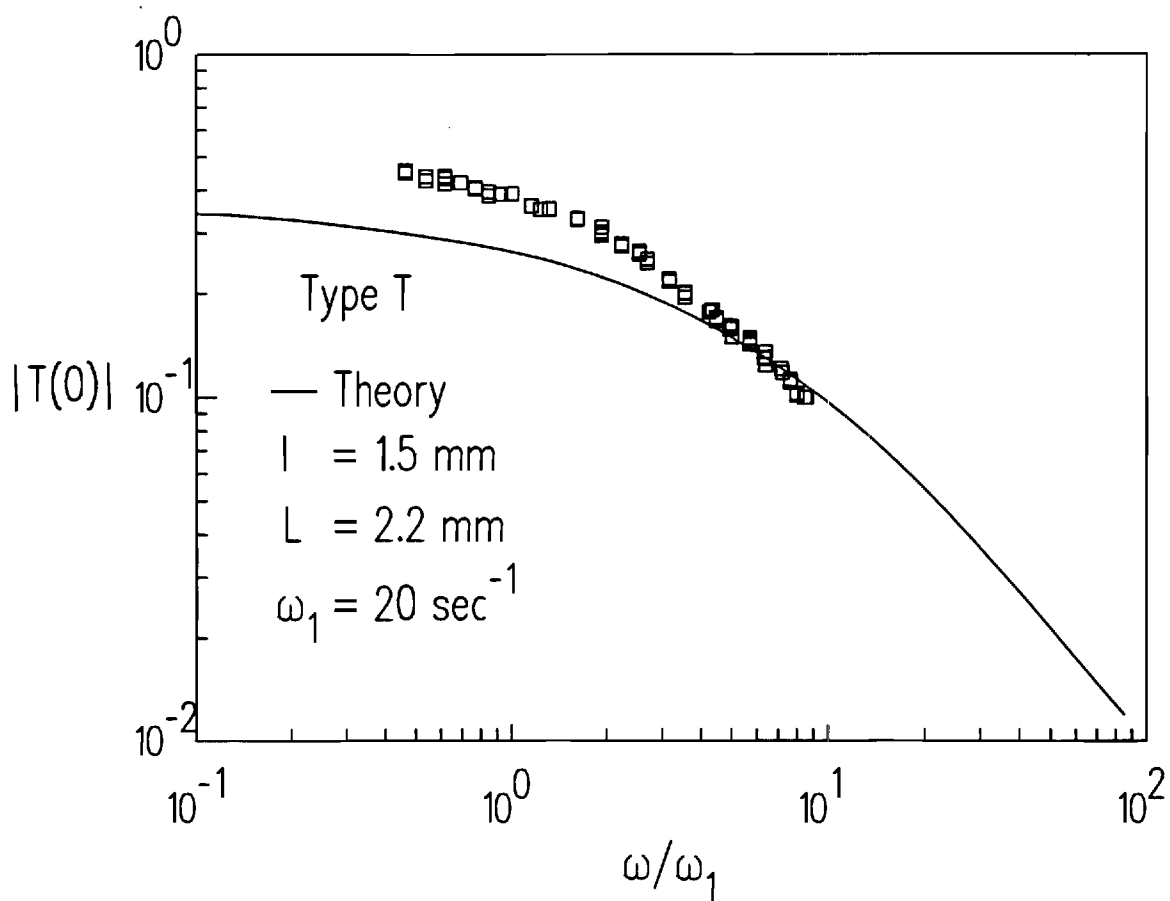
4. Photograph of a type T junction formed by laser heating. Diameter of wire is $76\mu\text{m}$.



6. Gas Temperature Profile



8. Amplitude Ratio and Phase Angle vs. Gas Temperature Frequency.
 Junction formed by Omega Engineering. Actual wire length: $l = 1.25 \text{ mm}$



10. Amplitude Ratio and Phase Angle vs. Gas Temperature Frequency for Thermocouple with Large Bead. Actual wire length: $l = 1.3 \text{ mm}$